




University of  
Stavanger

Faculty of Science and Technology

## MASTER'S THESIS

Study program/ Specialization:  Msc Offshore Technology/ Marine and Subsea Technology	Spring semester, 2015  Open access
Writer:  Gonzalo Diz-Lois Palomares	 ..... (Writer's signature)
Faculty supervisor:  External supervisor(s):	Bjørn Hjertager  Luca Oggiano
Thesis title:  CFD SIMULATIONS ON A PARTIALLY SUBMERGED CYLINDER UNDER REGULAR WAVES USING OPENFOAM®	
Credits (ECTS):  30	
Key words:  IhFoam, OpenFoam, InterFoam, Waves, Wave Forces, Wave structure interaction.	Pages: 52  + enclosure: -  Stavanger, 15 June 2015. Date/year



Universitetet  
i Stavanger



UNIVERSITY OF STAVANGER

MASTER THESIS PROJECT

**CFD SIMULATIONS ON A PARTIALLY  
SUBMERGED CYLINDER UNDER REGULAR  
WAVES USING OPENFOAM®**

---

*Author:*  
Gonzalo DIZ-LOIS PALOMARES

*UiS Supervisor:*  
Dr. Bjørn HJERTAGER  
*External Supervisor:*  
Dr. Luca OGGIANO

June, 13 2015

LaTeX inside

## **Abstract**

In this Master Thesis, an overview of the performance and applicability of IHFoam numerical tool to offshore engineering related problems is presented.

IHFoam is a recent numerical tool for wave modeling using a Computational Fluid Dynamics (CFD) approach, a set of boundary conditions for modelling of numerical wave tanks, compiled together within a well known CFD project, OpenFOAM®. This is being constantly developed by scientific research communities worldwide and is also stepping into the industry as a reliable and accurate tool providing solutions for multitude of engineering problems where fluids are present.

Different sets of simulations, picked from the literature or experimental tests, aim the validation of this tool: i) simple two dimensional simulations where the waveform is confronted against theoretical solutions, are tailored for validation of the model, and ii) three dimensional simulations are included for completeness in order to investigate the loads exerted to a vertical cylinder in the middle of a numerical wave flume.

# Preface

The aim of this Thesis report is a follow up of the research project initiated as a requirement for obtaining the MSc Offshore Technology, specialization of Marine and Subsea Technology, at the University of Stavanger, Norway.

This work will also serve as a kick off investigation in the UiS to start experiencing and assessing one of the main CFD codes modelling available as a research tool for wave structure interaction from a *a priori* general and unrestricted perspective, that is, OpenFOAM® environment compiled together with IHFoam routines.

This project will focus on assessing the performance of this specific CFD tool (IHFoam) for predicting wave parameters and forces. For this purpose, an assessment is made on the wave form  $\eta$ , the velocities and the forces on a simple submerged vertical cylinder, by simulating several setups covering a wide range of conditions.

# Contents

<b>1</b>	<b>Introduction</b>	<b>5</b>
<b>2</b>	<b>State of the Art</b>	<b>6</b>
2.1	Classical Wave Theory . . . . .	6
2.1.1	Assumptions and founding equations . . . . .	6
2.1.2	Linear Theory . . . . .	9
2.1.3	Non Linear theories . . . . .	9
2.1.4	Wave stability . . . . .	12
2.1.5	Wave Loads . . . . .	13
2.2	Numerical Methods . . . . .	14
2.2.1	Volume of Fluid Method for 2 phase flows . . . . .	15
2.2.2	Boundary Conditions . . . . .	16
2.2.3	Wave Generation . . . . .	17
2.2.4	Wave Absorption . . . . .	17
2.3	Previous works . . . . .	20
<b>3</b>	<b>Numerical Model Description</b>	<b>21</b>
3.0.1	Equations . . . . .	21
3.0.2	Boundary Conditions . . . . .	21
<b>4</b>	<b>Methodology</b>	<b>25</b>
4.1	Two dimensional simulations . . . . .	25
4.1.1	Domain . . . . .	26
4.1.2	Boundary Conditions . . . . .	27
4.1.3	Diffusive error . . . . .	27
4.1.4	Reflection coefficient . . . . .	28
4.2	Three dimensional simulations . . . . .	29
4.2.1	Domain . . . . .	30
4.2.2	Boundary Conditions . . . . .	30
<b>5</b>	<b>Results</b>	<b>32</b>
5.1	Two dimensional simulations . . . . .	32
5.1.1	Wave Generation . . . . .	32
5.1.2	Wave Propagation . . . . .	35
5.2	Three dimensional simulations . . . . .	40
5.2.1	Simulations from Paulsen et al. [2012] . . . . .	41
5.2.2	Experiments from Grue and Huseby [2002] . . . . .	41
5.2.3	Load cycle . . . . .	42
<b>6</b>	<b>Summary and Conclusions</b>	<b>48</b>
6.1	Further work . . . . .	50

# List of Figures

2.1	Representation of linear wave vs Stokes wave . . . . .	10
2.2	Summary of applicability of wave theories, from Méhauté [1976] . . . . .	12
2.3	Approximation of dispersion relation, from Luppés et al. [2010] . . . . .	19
3.1	Wave generation and boundary conditions . . . . .	23
4.1	Summary of cases and applicability of wave theories, from Méhauté [1976] . . . . .	27
4.2	Numerical Domain in 2D . . . . .	27
4.3	Numerical Domain in 3D . . . . .	30
5.1	Generation at inlet $H/L = 0.05$ . . . . .	32
5.2	Generation at inlet $H/L = 0.032$ . . . . .	33
5.3	Generation at inlet $H/L = 0.092$ . . . . .	33
5.4	Generation at inlet $H/L = 0.092$ refined . . . . .	33
5.5	Generation at inlet $H/L = 0.092$ setting $cAlpha=0$ . . . . .	34
5.6	Influence of compression in wave generation error . . . . .	35
5.7	Early breaking wave . . . . .	35
5.8	Example of linear reflections in the wave form . . . . .	36
5.9	Example of non linear reflections in the wave form . . . . .	36
5.10	Example of non linear effects at the outlet . . . . .	37
5.11	Distorsion of wave form due to non linearities . . . . .	37
5.12	Stationary waves in OC5 cases . . . . .	38
5.13	Reflection coefficient vs $\frac{d}{L}$ in 2D simulations . . . . .	38
5.14	Spurious velocities from residuals of the cancellation velocity . . . . .	39
5.15	Spurious velocities on the air phase just above the free surface . . . . .	39
5.16	Spurious air blows coming from the outlet boundary . . . . .	40
5.17	Plot of diffusive error (average value for 4 waves, as defined in 4.1.3) against $\frac{d}{L}$ . . . . .	40
5.18	Inline Forces for $D=6$ m, $H/H_{max}=0.6$ , $kd=0.85$ . . . . .	42
5.19	Inline forces for $D=6$ m, $H/H_{max}=0.6$ , $kd=1.2$ . . . . .	43
5.20	Inline force for $D=6$ m, $H/H_{max}=0.81$ , $kd=0.87$ . . . . .	44
5.21	Inline force for $D=6$ m, $H/H_{max}=0.82$ , $kd=1.22$ . . . . .	45
5.22	Inline force for $D=6$ cm, $H/H_{max}=0.634$ , $kd=3.05$ . . . . .	46
5.23	Inline force for $D=6$ cm, $H/H_{max}=0.653$ , $kd=4.53$ . . . . .	46
5.24	Example of loading cycle sequence for $D=6$ m, $T=11.35$ s, $H/H_{max}=0.82$ , $kd=1.22$ . . . . .	47

# List of Tables

4.1	Data sets considered for two dimensional simulations . . . . .	26
4.2	Boundary conditions for two dimensional simulations . . . . .	28
4.3	Data sets considered for three dimensional simulations . . . . .	30
4.4	Boundary conditions for three dimensional simulations . . . . .	31
5.1	Summary of errors in wave generation ( $\hat{\epsilon}_0$ ) and propagation at the midflume ( $\hat{\epsilon}_m$ ) . . . .	34
5.2	Summary of forces for Paulsen et al. [2012] cases . . . . .	41

# Chapter 1

## Introduction

In offshore conditions, environmental loads, and particularly those of waves, are usually a major concern driving the design process of marine structures. Waves, and wave loads in particular, are usually dealt with by means of analytical solutions obtained for very simple cases with limiting assumptions, the rest are usually modelled by reduced scale tests in experimental facilities tailored to model specific conditions. The former are usually too limited to model most geometries and load conditions, dynamic systems or wave structure interaction. The scale tests provide valuable input for the design process, but they are also limited in simulating the design conditions, geometry and loading, but also because some forces are not scalable –i.e. viscosity or surface tension – and the control of the boundary conditions is quite limited.

Moreover those tests require always a very complex setup, with costly facilities, and only limited geometries and loading conditions can be included, for economic reasons. For instance, ultra deep water offshore structures in the range of 1500- 2000 m depth, would require a basin depth of 30-50 m depth keeping usual scale factors of 1:50 or 1:70. This is something unthinkable nowadays, and so other techniques must be developed. Numerical simulation

Another set of tools is emerging as a promising complement to the aforementioned, the numerical simulations, these will –and are already – developing an important part in solving these issues. They are based on solving the foundational differential equations of the problem and its boundary conditions by means of numerical (discrete) methods. This requires the appropriate discretization schemes considering the variables that are relevant to the problem. The potential of this tool is tremendous since, in theory, all kinds of geometries, loadings, couplings and system behaviours can be modelled *a priori*.

The development of numerical simulations has to be thoroughly validated with experimental data, this has to be done starting from elementary wave structure interactions, like a partially submerged vertical cylinder subject to wave loading, and such is the aim of this work.



# Chapter 2

## State of the Art

In this chapter a brief review of the theoretical basis of the underlying concepts used in this document is presented. It is not intended to be a thorough insight, so it is focused on the theories, models, techniques and expressions required for getting to the results presented in chapter 5.

### 2.1 Classical Wave Theory

Gravity waves are a periodic perturbation originated at the interface between two different phases by a displacement of fluid out of the position of static equilibrium. Once the fluid is displaced, the free surface will try to restore its original position, oscillating between this equilibrium state (still water level) [Lig, 2001].

Historically wave models have been dealt with by means of different theories that imply certain specific assumptions. The very beginning of wave theory is the linear theory developed by Airy (1895) – also known as Stokes I theory – which basically considers a simple sinusoidal wave travelling in space and varying with time. By doing this, It also assumes potential theory for the calculation of the velocity field – i.e. no friction losses –and linearises the free surface boundary conditions and the differential equation itself (see ref. [Fenton, 1990] for details). This first approximation is valid for infinite depths, that is, when the wave is unaffected by the presence of the bottom  $-\frac{d}{L} > 0.5$ –and for cases when the steepness  $\epsilon = \frac{H}{L}$ , is sufficiently small and the linearisation is acceptable – i.e. very smooth waveforms. Those are the reasons why this first theory is called the *linear* theory or the small amplitude theory. From here, other theories will take into account some of the non linearities by including a series approximation of the free surface in terms of the steepness  $\eta = f(\epsilon)$ , in order to consider the non linearities due to the surface *kinematic* and *dynamic* boundary conditions, allowing to model steeper waves. Other sources of non linearities like breaking waves or velocity skewness and asymmetries, are not accounted for in most theories and none of them considers friction losses. The term *nonlinear* is a complex concept that includes a whole spectrum of behaviours that differ from the linear theory, but none of the wave theories captures those fully.

#### 2.1.1 Assumptions and founding equations

There are some common assumptions included the linear wave theory that strongly influences its accuracy and applicability. The main assumption of incompressibility is very convenient when dealing with water, and no drawbacks can be pointed out here. This assumption will lead to a very compact equation for the velocity:

$$\nabla \cdot \vec{U} = 0 \tag{2.1}$$

Another assumption is the existence of a potential function  $\phi$ – associated to a conservative scalar field <sup>1</sup> such as the gravitational field – that governs the velocity relies on the irrotationality:

$$\vec{\omega} = \nabla \times \vec{U} = \vec{0} \quad (2.2)$$

Furthermore, the potential theory provides an elegant relation to obtain the velocities from the potential function  $\phi$ :

$$\vec{U} = \frac{\partial \phi}{\partial x} \cdot \vec{i} + \frac{\partial \phi}{\partial y} \cdot \vec{j} + \frac{\partial \phi}{\partial z} \cdot \vec{k} \quad (2.3)$$

Both equations 2.1 and 2.3 combined together lead to the Laplace equation, known to be a linear differential operator, which is very convenient:

$$\nabla^2 \phi = 0 \quad (2.4)$$

The main drawbacks of embracing the potential theory are related to i) neglecting the friction losses, which can be relevant for long domains and shallow waters and/or for breaking conditions, and ii) the implied irrotationality, which keeps the model from modelling rotating flows, like eddies or swirls. This, though, is quite assumable condition in waves if they are non breaking, that is why all relevant theoretical studies in wave hydrodynamics are formulated by means of irrotational flow. One of the consequences of irrotationality is that the waves are symmetrical about the wave crest. In steep waves, though, where the wave is close to breaking, this assumption is on its limit and the theory needs some adjustments to account for the inaccuracies arisen from some rotationality according to Mas [2007].

The boundary conditions for the potential theory can be classified as *linear* and *nonlinear*:

1. Linear boundary conditions are those having just linear differential operators in their definitions, for instance, a Dirichlet boundary condition for the velocity, such as normal velocity to a wall  $v_n = 0$ , this, in terms of potential variable, leads to:

$$\frac{\partial \phi}{\partial n} = 0 \quad (2.5)$$

2. Non linear boundary conditions, these are defined in terms of non linear differential operators or coupled variables– i.e. a definition of the boundary condition that is referring to the solution  $\eta(x, t)$ .

This latter type is the case of the so called *kinematic boundary condition*, this condition states that the flow cannot trespass certain boundaries or walls, which in a flat bottom leads to eq. 2.5, but when dealing with the moving and irregular free surface, and the material derivative concept is used –  $\frac{DF}{Dt}$  along a moving particle – the expression obtained is:

$$\frac{\partial}{\partial t} (z - \xi(x, y, t)) + \nabla \phi \cdot (z - \xi(x, y, t)) = 0 \quad (2.6)$$

---

<sup>1</sup>A conservative field is a escalar field where the work needed to displace a particle is independent on the path followed, for instance, magnetic, electric or gravitational fields.

Yielding to:

$$\frac{\partial \eta}{\partial t} + \frac{\partial \phi}{\partial x} \frac{\partial \eta}{\partial x} + \frac{\partial \phi}{\partial y} \frac{\partial \eta}{\partial y} - \frac{\partial \phi}{\partial z} = 0, z = \eta(x, y, t) \quad (2.7)$$

Which is highly non linear, since it refers to the solution  $\eta(x, y, t)$ .

Another necessary non linear boundary condition states that the pressure at the free surface is the same as the atmospheric, this is the so called the *dynamic boundary condition*. This condition can be obtained manipulating the Bernoulli Energy Equation for irrotational and potential flows.

$$g \cdot \eta + \frac{\partial \phi}{\partial t} + \frac{1}{2} \cdot \left( \left( \frac{\partial \phi}{\partial x} \right)^2 + \left( \frac{\partial \phi}{\partial y} \right)^2 + \left( \frac{\partial \phi}{\partial z} \right)^2 \right)_{z=\eta(x,y,t)} = 0 \quad (2.8)$$

The solution has the form:

$$\eta = -\frac{1}{g} \left( \frac{\partial \phi}{\partial t} + \frac{1}{2} \nabla \phi \cdot \nabla \phi \right), z = \eta(x, y, t) \quad (2.9)$$

Therefore, both the dynamic and kinematic boundary condition are sources of non linearities in the problem. Note the mixed terms in both expressions where the potential  $\phi$  is together with the free surface elevation  $\eta$ , being both coupled unknowns.

Nevertheless, those expressions can be fully linearised to get a compact and simple solution. Another alternative is that they can be developed in Taylor series around the still water elevation ( $z=0$ ) by means of a small parameter – for instance, the wave steepness  $\varepsilon = \frac{H}{L}$ . This expansion series can be truncated to obtain an analytical approximation for steeper waves. That is the procedure for obtaining the higher order Stokes solutions.

Another important boundary condition is that of the inlet and outlet boundaries in a wave tank, these are not treated in classical wave theory, since they come from the numerical integration problem of a closed domain from a CFD point of view. On the one hand, at the inlet, the correct conditions for water elevations and velocities should be specified with time, on the other hand, the outlet –and inlet –boundaries should act as *transparent* walls, this can turn into a difficult problem and there is not a single way of treating this issue. We will discuss further when we start discussing the properties of the numerical model.

In general, those conditions can have the form [Fenton, 1990]:

$$\frac{\partial \phi}{\partial x} = G(x, y, z, t) \quad (2.10)$$

Where  $G(x, y, z, t)$  is an known velocity field at the outlet.

## 2.1.2 Linear Theory

The linear theory implies a full linearisation of the dynamic and kinematic boundary conditions, together with eq.2.4:

$$\nabla^2\phi = 0; \text{ in } \Omega \quad (2.11)$$

$$\frac{\partial\eta}{\partial t} = \frac{\partial\phi}{\partial z}; \text{ at } z = 0 \quad (2.12)$$

$$\frac{\partial\phi}{\partial t} = -g\eta; \text{ at } z = 0 \quad (2.13)$$

$$\frac{\partial\phi}{\partial z} = 0; \text{ at } z = -d \quad (2.14)$$

The Airy wave has the following form:

$$\eta = \frac{H}{2}\cos(k \cdot x - \omega \cdot t + \theta) \quad (2.15)$$

Where  $H$  is the wave height,  $k = \frac{2\pi}{L}$  the wave number,  $\omega$  the angular frequency,  $x$  is the spatial variable (in one dimension),  $t$  is the time variable and  $\theta$  is some initial phase (usually set to 0, only relevant when there is interaction with other waves). This wave is fully linear and symmetric from the still water level.

From eqs eqs. (2.11) to (2.14) the exact expression can be derived for the potential:

$$\phi = \frac{H \cdot g}{2 \cdot \omega} \frac{\cosh(k(d+z))}{\cosh(kd)} (k \cdot x - \omega \cdot t) \quad (2.16)$$

From this expression, the other relevant parameters, such as velocities and accelerations, can be derived through eq.2.3.

## 2.1.3 Non Linear theories

### Stokes Waves

A generalisation of the linear theory is made in the higher order theories. As it has been already mentioned, there are different theories depending on the approach to solve eq. 2.4 and the kinetic and dynamic boundary conditions.

A step forward from the Airy wave is that of the Stokes higher order waves. Higher order Stokes theory is basically a generalization of the linear theory by including  $n$  harmonics when defining the free surface  $\eta$ :

$$\eta = \sum_{i=1}^n \eta_i = \sum_{i=1}^n A_i \cdot \epsilon^{n-1} \cos(i(k \cdot x - \omega \cdot t)) + \Theta(\epsilon^n) \quad (2.17)$$

$n$  here is the *order* of the Stokes wave and  $\Theta(\epsilon^n)$  is a truncation error of order  $\epsilon^n$ .

Each of the components of the Stokes wave  $\eta_i$  has double the frequency from the one with lower order, and their amplitudes  $A_i$  can be obtained by applying the kinematic and dynamic boundary

conditions expressing the non linear contributions by the Taylor expansion series of order  $n$  – the so called *Stokes expansion*. For instance, second order theory can be obtained by expressing the dynamic boundary conditions in a Taylor series of order 2:

$$\frac{\partial^2 \phi}{\partial t^2} + g \frac{\partial \phi}{\partial z} + 2 \nabla \phi \cdot \nabla \frac{\partial \phi}{\partial t} - \frac{1}{g} \frac{\partial \phi}{\partial t} \frac{\partial}{\partial z} \left( \frac{\partial^2 \phi}{\partial t^2} + g \frac{\partial \phi}{\partial z} \right) = 0 + \Theta(\phi^3) \quad (2.18)$$

Similarly, with the kinematic boundary condition 2.9:

$$\xi = \frac{1}{g} \left( \frac{\partial \phi}{\partial t} + \frac{1}{2} \nabla \phi \cdot \nabla - \frac{1}{g} \frac{\partial \phi}{\partial t} \frac{\partial^2 \phi}{\partial z \partial t} \right)_{z=0} + \Theta(\phi^3) \quad (2.19)$$

This will give us the following solution with 2 harmonics, for a Stokes wave of second order.

$$\eta = A \cos(kx - \omega t) + \frac{1}{2} k^2 A^2 \cos(2(kx - \omega t)) \quad (2.20)$$

The coefficients of the Stokes waves have been obtained up to the fifth order wave, with very long expressions that are out of the scope of this section.

Since the order of magnitude of the individual terms of the Stokes expansion are assumed to be in the order of  $\Theta(\frac{d}{L}) = 1$ , a problem occurs if  $\frac{d}{L} \ll 1$ , where secondary crests begin to appear in the wave through. In practice it is required that  $\frac{d}{L} > 0.10 - 0.15$  to avoid this problem for a Stokes 5<sup>th</sup> wave [Fenton, 1990].

Stokes waves break with the horizontal symmetry of the wave form in respect to the still water level, creating higher crests and shallower troughs as can be observed in fig. 2.1. This produces steeper crests and more impact-like forces than linear waves, as will be seen in chapter 5.

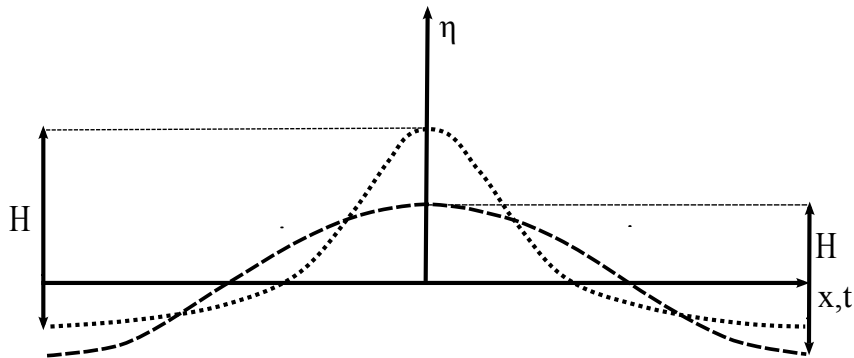


Figure 2.1: Qualitative representation of a linear wave form (dashed) vs Stokes wave (dotted)

Stokes theory is more suitable for waves that are not very long relative to the water depth (ref [Fenton, 1990]) and when used out of their suitable limits, will fail to converge or converge very slowly. To overcome this, Dean (1965) proposes a solution to the given eq.2.4 by producing series expansions based on a small parameter and obtaining the solution numerically using a spectral approach. This path leads to the so called *stream function* theory developed by [Fenton and Rienecker, 1982]. In this case it is more convenient to use the stream function as the main variable to solve, from

which all the others (velocities, pressure) will be obtained.

## Stream Function Theory

The classic approach underlying the different wave theories has been that of Stokes', that is, solving the differential equation of the potential 2.4 and the suitable boundary conditions approximated to a given order by means of the Taylor expansion series around  $z = 0$ , by this we can obtain an analytical expression for the amplitudes of the different harmonics  $\eta_i$ . An alternative to this is obtaining the harmonic coefficients by means of a Fourier transform directly, solving the equations for the reference variables numerically –by Newton's method, for instance. That is the approach underlying behind the *Stream Function* theory derived by [Fenton and Rienecker \[1982\]](#).

This theory relies on the existence of a stream function  $\psi$  that fulfils:

$$-\frac{\partial\psi}{\partial x_r} = v \quad (2.21)$$

$$\frac{\partial\psi}{\partial z} = u \quad (2.22)$$

$$(2.23)$$

Where  $x_r$  is the spatial horizontal coordinate in the plane of the wave motion, moving with the wave velocity  $c$  at the top of the wave crest.  $z$  is the vertical coordinate.

The condition for its existence is incompressibility (eq. 2.1), combining this with irrotationality, Laplace equation for incompressible fluids turns into:

$$-\frac{\partial^2\psi}{\partial x_r^2} + \frac{\partial^2\psi}{\partial z^2} = 0 \quad (2.24)$$

From here, Dean (1965) used this definition to create a new approach to solve eq. 2.24 with respect of the coordinate system  $(x_r, z)$ .

The general form for the stream function considered in this theory is:

$$\psi(x, z) = B_0 z + \sum_{j=1}^N B_j \frac{\sinh jkz}{\cosh jkh} \cosh jkx \quad (2.25)$$

The coefficients are obtained by a Fourier transform, solving the equation 2.4 in the frequency domain.

This theory is a convenient approach for a wide range of depths, since its assumptions don't impose limitations to the parameters  $d/L$  or  $H/L$  for convergence, in contrast with Stokes and Cnoidal theories. Its wave form will adapt fairly well to any particular condition (in the range of wave parameters where waves are stable) [[Fenton, 1990](#)] and it can be particularly useful for regular steep waves in shallow water.

Other non linear theories, such as Bousinesq's solitary wave or *Cnoidal* waves, are based on the same principle as the stream function theory, that is, posing the problem in terms of the stream function and then solving it by approximation of the variables by expansion series by means of a small parameter (just like Stokes' approach), in this case, the expansion parameter is  $H/d$ . Those are limited to long and smooth waves.

## 2.1.4 Wave stability

Each wave theories are numerically stable for a certain range of parameters, except for the stream function theory, which is a general approach to the problem. As stated previously, linear waves are limited both by the wave steepness and the water depth, applicability of Stokes waves is limited mainly by the relative wave depth  $d/L$ .

The applicability of the different wave theories are summarized in figure 2.2. The suitability for the different theories is shown, depending on the depth – adimensionalized by the period  $\frac{h}{gT^2}$  – and the steepness of the waveform – taken here into account with the dimensionless parameter  $\frac{H}{gT^2}$ .

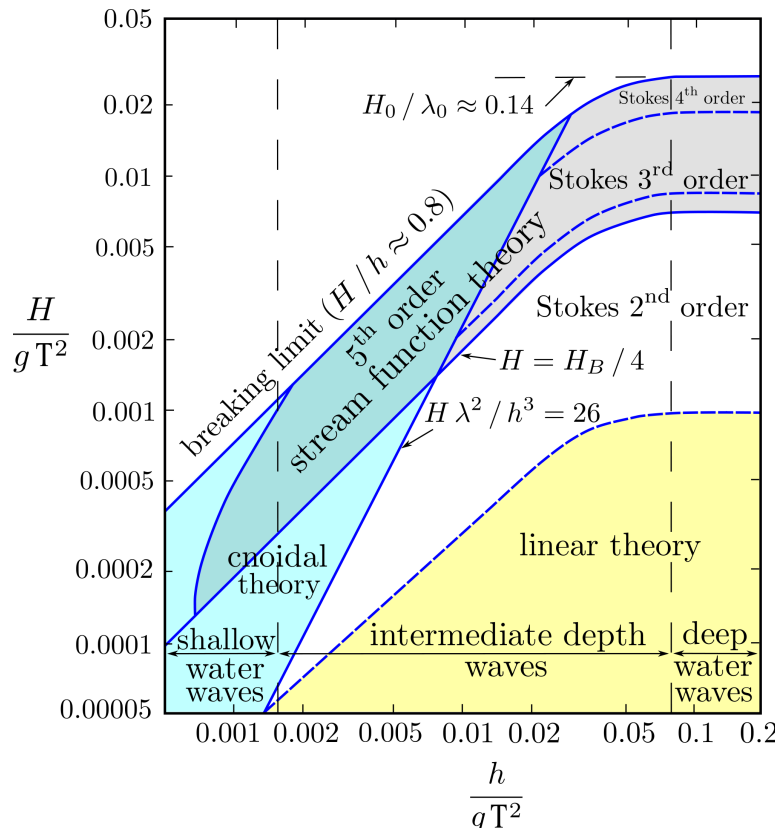


Figure 2.2: Selection of suitable wave theories, taken from Méhauté [1976].  $H$  is the wave height,  $h$  is the water depth,  $\lambda$  is the wave length and  $T$  is the wave period

A slightly different issue than the wave theory numerical stability is the physical wave stability. Wave forms in a real environment will be limited by a number of factors, namely:

- Water depth: Shallow water will make the wave feel the bottom, the energy of the wave is constrained in a more limited water column, increasing the wave height, but also reducing wave length, and thus increasing wave steepness. More over, troughs tend to be longer than crest –developing a pronounced asymmetry in the horizontal axis – so the local wave steepness at the crest area grows dramatically. This, taken to the limit, induces the collapse of the wave form, i.e. breaking of the wave.
- Sometimes non linear effects, such as wind blowing on the water surface or opposing currents, can create temporarily high steepness wave forms, which might be unstable and breaking, even in very deep water.

- Other situations, such as the presence of an obstacle or structure, reflected waves or non linear superposition of waves, can add steepness to  $\eta$  and induce breaking.

All those factors will limit the possible combinations of  $H$ ,  $L$  and  $d$  that one may encounter in real gravity waves. [Fenton, 1990] and Williams [1981] derived a theoretical expression from the Stokes wave theory for the maximum wave height that is stable given the depth and the wave length (see eq. 2.26).

$$\frac{H_{max}}{d} = \frac{0.141063 \frac{L}{d} + 0.0095721 \left(\frac{L}{d}\right)^2 + 0.0077829 \left(\frac{L}{d}\right)^3}{1 + 0.0788340 \frac{L}{d} + 0.0317567 \left(\frac{L}{d}\right)^2 + 0.0093407 \left(\frac{L}{d}\right)^3} \quad (2.26)$$

### 2.1.5 Wave Loads

An analytical expression exists for wave loading on vertical cylinders. The hydrodynamic forces on a piled structure is usually calculated by means of the Morison equation, eq. 2.27

$$f(z,t) = \rho \pi C_M \frac{D^2}{4} \frac{du}{dt} + \rho C_D u^2 D \quad (2.27)$$

Where  $f(z,t)$  is the total force per unit of length of the pile,  $z$  is the vertical coordinate,  $\rho$  is the density of the fluid,  $C_M$  is the mass coefficient (usually taken equal to 2 for cylinders),  $D$  is the diameter of the submerged cylinder (can be  $z$  dependent),  $u$  is the horizontal velocity normal to the cylinder, and  $C_D$  is the drag coefficient, dependent on the Reynolds number  $Re$ . the first term responds to the inertia forces, the second term represents the contribution of drag forces.

The relevance of the drag and inertia terms is usually assessed by means of the *Keulegan-Carpenter* number, named after Garbis H. Keulegan (1890–1989) and Lloyd H. Carpenter:

$$N_{KC} = \frac{u_0 T}{D} \quad (2.28)$$

Where  $u_0$  is the amplitude of the wave velocity –the particle velocity at the wave crest–  $T$  is the wave period and  $D$  is the diameter of the cylinder.

The number is a relation between the convective acceleration ( $(u \cdot \nabla) u \sim \frac{V^2}{L}$ ) and the local acceleration ( $\frac{\partial u}{\partial t} \sim \frac{V}{T}$ ) as derived from the dimensionless form of the Navier Stokes equations.

When  $N_{KC}$  is small, we either have that  $u_0 T$  is small or  $D$  is large. The first possibility implies that the oscillations of flow around the cylinder are slow and there is no flow separation. The second possibility implies that we do not have too many eddy currents generated. For both cases, the inertia forces will dominate.

The limits for the inertia dominated cases are somehow diffuse, the flow separation for two-dimensional oscillatory flow around vertical cylinders occurs around  $N_{KC} = 1.6$ , nevertheless Sumer and Fredsø [2006] proposes  $N_{KC} \ll 20 - 30$  for considering a inertia dominated flow. In this project  $N_{KC} = [7.565 - 10.73]$ , which is considered well into the aforementioned range to assume inertia dominated flow.

Equation 2.27 is more a semi empirical expression than a result of equilibrium analysis. Therefore it considers a series of coefficients that depend on the characteristics of the object (roughness, size, shape, ...) and the flow conditions (Reynolds number, boundary conditions, proximity of walls, ...).



The velocities and accelerations can be obtained from a suitable theory and used as an input for the given eq. 2.27.

Some requirements need to meet for applying eq. 2.27:

- Constant velocity/acceleration over a certain part of the wave. This means that the diameter of the structure has to be small in comparison with the length of the wave, approximately:  $D < L/5$ . If the structure is wider or the wave is shorter, the Morison approximation that assumes that there is a period with constant velocity and acceleration is no longer true, and the terms for drag and inertial forces are not valid, since they are both based on this assumption.
- Non breaking wave at the cylinder/structure. The terms for the Morison equation assume a smooth change in forces (both for dynamic pressure (velocity) and inertial forces (acceleration)). A breaking wave has completely different dynamics, since slamming of water occurs against the wall of the structure so a sudden impact load strikes the structure producing great turbulence, even compressed air trapped inside the wave shape can hit the structure. In this conditions, a slamming factor  $C_s$  can be introduced to take this into account in the Morison expression. This factor is ranging from  $[\pi - 2\pi]$  which depends largely on the wave form.

Breaking waves usually happen when the waveform is too steep or the depth is too shallow, or even in unusual cases, as strong wind blowing or current against the wave (artificially increasing its steepness).

- The structure should not move considerably when the waves hit, this is stated as:  $s < 0.2D$ , where  $s$  is the displacement and  $D$  is the diameter of the structure. If this limitation is violated, dynamic forces and coupled motions such as vortex induced vibrations actuate on the structure, and the acting forces cannot just be modelled as the sum of drag and inertial forces. This limitation is not very strict for stiff structures, but could be a concern in slender pipes such as risers or flowlines.
- Other assumptions, such as the considerations on  $C_D$  (its dependency with Reynolds number or with roughness or the shape of the structure) are also relevant but largely out of the scope of this project.

## 2.2 Numerical Methods

CFD is a branch of the Fluid Mechanics that uses numerical methods for modelling fluid flows resolving the Navier Stokes Equations (NSE). These equations, properly discretized, together with the appropriate boundary conditions, both in time and in space, and a meshed domain, form a complete posed problem for the CFD analysis.

CFD can be seen as a multidisciplinary topic though, a shared knowledge of Fluid Mechanics, computer science and numerical analysis. In this thesis, focus is set to its application to the Marine technology (Fluid Mechanics) side, leaving the computer science and numerical discretization point of view for further specialised work.

The CFD discipline started in los Alamos (CA,US) after the Second World War but didn't become mainstream until the mid 70's in the XX century. It has turned into a common tool in fluid analysis during the last 20 years, developed together with the constant increase in data processing power of available computers. Nevertheless, its application to waves hasn't started until recent times, with

the appearance of new specific solving techniques, boundary conditions and the availability of calculation power. This context allowed for the analysis of the wave problem in a general form, starting from the NSE.

The NSE is a general set of equations for fluids and are the very foundation of the CFD. They are obtained applying continuity equation and Newton's second law of motion together with the assumption that the stress tensor is a sum of a viscous –deviatoric– tensor and a spheric pressure gradient tensor (the so called *constitutive relation*):

$$\underline{\sigma} = -p\underline{\underline{I}} - \frac{2}{3}\mu(\text{tr}\underline{\underline{D}})\underline{\underline{I}} + 2\mu\underline{\underline{D}} \quad (2.29)$$

Where  $\underline{\sigma}$  is the stress tensor,  $p$  is the pressure (scalar),  $\mu$  is the kinematic viscosity,  $\underline{\underline{I}}$  is the unity tensor and  $\underline{\underline{D}}$  is the strain rate tensor.

The general NSE equations can then be expressed in the following compact form:

$$\frac{\partial \rho}{\partial t} + \nabla \cdot (\rho \vec{U}) = 0 \quad (2.30)$$

$$-\nabla p + \mu(\nabla^2 \vec{U}) + \frac{1}{3}\mu(\nabla \cdot \vec{U}) + \rho b = \rho \dot{U} \quad (2.31)$$

These equations are suitable for non turbulent flows, but can be generalized including turbulence if the turbulent variables  $-p$  and  $\vec{U}$  are averaged through time. They won't be shown here, since the scope of this document is restricted to laminar simulations.

### 2.2.1 Volume of Fluid Method for 2 phase flows

The Volume of Fluid Method (VOF) is a technique developed by [Hirt and Nichols \[1981\]](#) and modified by for two phase flows by [\[Berberović et al., 2009\]](#). It mainly consists on using an approximation when modelling the interface of two immiscible and incompressible phases, this is done by including a scalar variable  $\alpha$  in the equations that represents the portion of a volume of fluid –i.e. an infinitesimal volume in a differential equation and a cell volume if we deal with discrete equations – that is filled with one of the two phases (water in our case). The  $\alpha$  field is bounded between 0 and 1, so if, for instance,  $\alpha = 0.25$  this would mean that the cell is filled with water in a proportion of 25%. The method is implemented together with the RANS equations for incompressible flows by adding a equation of scalar transport for  $\alpha$  as showed in eqs. (2.32) to (2.34) (as showed in [Higuera et al. \[2013\]](#)).

$$\nabla \cdot U = 0 \quad (2.32)$$

$$\frac{\partial \rho \vec{U}}{\partial t} + \nabla \cdot (\rho \vec{U} \vec{U}) - \nabla \cdot (\mu_{eff} \nabla \vec{U}) = -\nabla p^* - \vec{g} \vec{r} \nabla \rho + \nabla \vec{U} \cdot \nabla \mu_{eff} + \sigma \kappa \nabla \alpha \quad (2.33)$$

$$\frac{\partial \alpha}{\partial t} + \nabla \cdot \alpha \vec{U} + \nabla \cdot \alpha \vec{U}_c (1 - \alpha) = 0 \quad (2.34)$$

Where  $\vec{U}$  is the Eulerian velocity,  $\vec{g}$  is the acceleration of gravity,  $p^*$  is a pseudo-dynamic pressure,  $\vec{r}$  is the position vector,  $\sigma$  is the surface tension and  $\kappa$  is the free surface curvature.  $\mu_{eff}$  is the *efficient dynamic viscosity*, which takes into account the molecular dynamic viscosity and the turbulent effects by means of the turbulent kinetic viscosity  $\nu_{turb}$ , see eq. 2.35.

$$\mu_{eff} = \mu + \rho \nu_{turb} \quad (2.35)$$

Equation 2.34 models the scalar transport of  $\alpha$ , which includes a material derivative plus an artificial compression term  $\nabla \cdot \alpha \vec{U}_c (1 - \alpha)$  [Weller, 2002] to have non zero values only at the free surface.  $\vec{U}_c = \min[c_\alpha |U|, \max[|U|]]$  where  $c_\alpha$  is a compression coefficient between 0 and 1. The compression term is zero if the velocity  $\vec{U}_c$  is perpendicular to the interface. The purpose of this compression of the velocity is to avoid smearing and diffusion of the free surface during simulations, potentially leading to a still water surface. This point is specially relevant for long simulations ( $\geq 50$  periods) as stated by [Afshar, 2010]. Without this numerical technique this diffusion can only be retarded if the mesh resolution is increased.

Equation 2.34 is solved by a specially designed solver within IHFoam called MULES (Multidimensional Universal Limiter for Explicit Solution) which ensures a final value with physical meaning – i.e. bounded between 0 and 1.

VOF technique allows to express any of the properties at every point in the domain by means of a single analytical expression. This is done by simply weighting the properties of the two phases in relation to their proportion  $\alpha$ . For instance, the density can be expressed as:  $\rho = \rho_w \cdot \alpha + \rho_a \cdot (1 - \alpha)$ , where  $\rho_w$  and  $\rho_a$  are the densities of the fluid and the air phases.

The VOF method allows complex configurations of the free water surface without the need of including a dynamic mesh, which is far more complex and less robust. There are some drawbacks though, and those are due to the fact that i) the VOF method doesn't perform well when there is high surface tension involved, which is not the case for gravity waves with long lengths, and ii) the VOF could be giving wrong results for high steepness of the free surface ( $H/L > 0.05$ ) according to [Afshar, 2010], but this is largely dependent on the compression factor  $c_\alpha$ . This latter issue has been observed in the simulations analysed in this project when using the compression technique for the alpha field transport equation 2.34 (see 5 for more details).

The VOF numerical model can support all available turbulence models in OpenFOAM®, namely:  $\kappa - \epsilon$ ,  $\kappa - \omega$ , *SST* and *LES*.

### 2.2.2 Boundary Conditions

The boundary conditions for the CFD approach need to be specifically tailored to the RANS equations with the VOF approximation. Since the definition of the problem is made from a more general perspective, they are different than the boundary conditions set for traditional wave theory.

There is no such thing as potential theory in the context of the RANS equations, but similar assumptions can be made, neglecting friction losses at boundaries, and assuming no turbulence –i.e. laminar flow. With this in mind, we can expect similar results from a CFD approach than from wave theory. Moreover, if the Keulegan-Carpenter number is in the range of  $N_{KC} \ll 20 - 30$ , we can expect an inertia dominated situation, as defined in subsection 2.1.5, where drag forces can be neglected. If we calculate the loads by integrating the normal pressure around the cylinder, neglecting the shear stresses – which are around zero, since the boundary condition for the wall is a slip condition – those loads should agree well with measurements.

Following this logic, slip conditions have been considered for all boundaries and objects in the simulations, meaning that only the normal velocity is set to zero on that surface.

Following is a short description of the specific boundary conditions for velocity:

### 2.2.3 Wave Generation

Wave generation in physical wave tanks can be challenging, the generation is made with wave makers that can be of a piston or flap type. Therefore wave boards cannot accurately reproduce the exponential velocity profiles of progressive waves, creating spurious waves together with the waves that are intended to create, namely: freely propagating waves, bound waves and evanescent waves [Wellens, 2012].

Unlike physical wavemakers, numerical wave generation can be achieved by imposing the exact theoretical velocity profile with a Dirichlet boundary condition, so spurious waves can be *a priori* avoided. The velocity profile is obtained from an analytical wave theory, choosing one that is suitable for the range of conditions of the experiment (see 2.2).

### 2.2.4 Wave Absorption

In this whole subsection we will follow the description of wave absorption based on Wellens [2012].

Waves are usually modelled to predict their behaviour and effects on open sea conditions, nevertheless, testing is always done in the controlled conditions of a laboratory. This has clear advantages, since in the open sea it is not possible to control basic parameters such as the incoming waves, the depth, wind, ... Nevertheless, this has a big drawback relative to the difficulty of imposing transparent boundaries at the outlet, this affects both physical experiments and numerical simulations.

The energy flux, travelling with the wave, has to leave the flume, if not, the reflections will affect the waves upstream and the basic parameters of the waves, giving misleading results.

#### Physical Wave Tanks

In a physical wave tank the problem is usually solved partially including absorbing elements such as porous media (*sponge layers* like gravel or gratings) dissipating the wave energy by increasing turbulence, or *absorbing beaches* (sloping bottoms), where the energy dissipation is due to friction with the bottom and the wave breaking turbulence, or a combination of the two. This approach to the problem is called *passive absorption*. These devices are usually can lead a reflection coefficient of up to 10%, for a well designed passive absorber [Edinburgh Designs Limited].

Another different philosophy is what is called *active absorption*, which consists mainly in controlling the reflections by means of the motion of the wave boards. This approach can be viewed from 3 different perspectives: [Schäffer and Klopman, 2000]:

1. Reversing time: the absorption of a wave can be seen as the opposite action of generating the same wave. Imposing an opposite motion in the paddles can, in theory, absorb the incident waves. This needs a measurement of the incoming waves and a controlling system so the paddles are moved to counteract the reflected velocities.
2. Cancelling the reflected wave using the superposition principle: The reflected progressive wave can be cancelled creating a wave of equal amplitude and opposite phase. Both waves will add so to cancel each other's velocity fields.
3. Creating a transparent boundary at the outlet, letting the waves propagate through it and leave the flume without reflections.

## Numerical wave tanks

The problem is the same in the context of a numerical simulation, but the approach has to be different. Numerically mimicking the effect of a given physical absorption element by accurately reproducing breaking wave conditions, friction and turbulence is unachievable today, and would be extremely costly in terms of computational resources and time. In turn, the approaches for dealing with numerical reflections are included within either one of this 3 methods:

1. Dissipation zones: The aim of this philosophy is reduce the wave energy before they actually reach the outlet boundary, so in theory no reflection can happen. A well known example is the pressure damping technique, which includes an artificial increased pressure term in RANS equations:

$$p = \alpha(x) \cdot w(x,t)|_{\eta} \quad (2.36)$$

Where  $p$  is the pressure variable,  $\alpha(x)$  is a coefficient that is gradually increased along a dissipation zone to increase the damping and  $w(x,t)|_{\eta}$  is the vertical velocity at the free surface.

This method is more efficient with short steep waves, where the vertical velocities are greater for long waves, longer zones are required to dissipate all the wave energy.

This numerical technique requires of damping (or dissipation) zones of 2 or 3 times the wavelength, according to [Wei and Kirby \[1995\]](#), which can be even larger than the domain itself, increasing the computational cost. Another important drawback is that some authors have also noticed an increase in the mean water level when using this dissipation zones [[Mendez et al., 2001](#)]. Another drawback stated by [Wellens \[2012\]](#) is that, at the inlet, they cannot dissipate outgoing waves and leave incoming waves unaffected at the same time.

2. Kinematics from external methods: The concept here is obtaining the solution of the waveform by means of external solvers, if there are differences with the solution in the internal method a local boundary condition – specific for a given simulation – is set to match the external solution. This is feasible if the conditions of the simulation can hold an undisturbed wave. Nevertheless, since the aim of the simulation is often modelling wave-structure interaction, the wave will be disturbed by the presence of the structure, this makes this procedure hard to apply. Some authors have suggested incorporating the effects of radiation and diffraction obtained from linear theory into this type of boundary condition to overcome this issue. This alternative is not so straight forward though, since non linear kinematics should be used for this purpose and there is not a non linear analytic theory that accounts for diffractions, as stated by [Wellens \[2012\]](#).
3. Non-reflective boundary conditions: They are also known as artificial boundary conditions, radiation conditions, absorbing boundary conditions or weakly reflective boundary conditions. They consist on solving a differential equation transformed to the frequency domain, solving this transformed equation and transforming the solution of the wave modes back into the time domain to obtain the operator. Getting a global solution –for all the frequency domain – is complex and costly so the boundary condition is approximated, being only valid for a range of frequencies around the harmonics of the solution. The solution is also truncated to a finite number of harmonics to save computational cost.

This latter type –Non-reflective boundary conditions– is the type implemented in IHFoam absorbing boundary condition. The cornerstone of this active absorption boundary condition is the so

called Sommerfeld radiation condition, for the potential in two dimensions:

$$\left( \frac{\partial^2}{\partial t^2} - c^2 \nabla^2 \right) \Phi = 0 \quad (2.37)$$

Applying a Fourier Transform to this equation to have it terms of frequency leads to the dispersion relation. Following linear theory and neglecting non linearities, any free surface elevation can be represented by a linear superposition of waves –the so called superposition principle – we can expand the dispersion relation in series, truncate the result and then doing an inverse Fourier Transform to have it back again in time, leading to this simplified form:

$$\left( \frac{\partial}{\partial t} + c \frac{\partial}{\partial x} \right) \phi = 0 \quad (2.38)$$

If we include the exact expression for the dispersion relation to obtain  $c$  we obtain a condition that is perfectly absorbing for a single component of the wave, since the dispersion relation has been truncated to just represent one of them:

$$\left( \frac{\partial}{\partial t} + \sqrt{gd} \sqrt{\frac{\tanh(kd)}{kd}} \frac{\partial}{\partial x} \right) \phi = 0 \quad (2.39)$$

Luppès et al. [2010] introduces an approximation to the dispersion relation so to represent not just one harmonic of the free surface, but all the components, this is done only to an acceptable range. A proper election of the coefficients  $a_0$ ,  $a_1$  and  $b_1$ , would give a reasonable approximation of  $c$  for a specified range, tailored to the most energetic harmonics of the incident waves. The approximate expression is shown in eq. 2.40 and its graphical representation in fig. 2.3.

$$c \approx \sqrt{gd} \frac{a_0 + a_1 (kd)^2}{1 + b_1 (kd)^2} \quad (2.40)$$

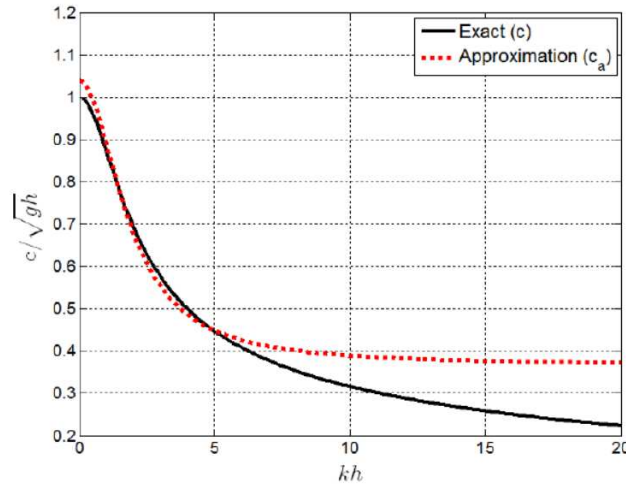


Figure 2.3: Approximation of the dispersion relation introduced in Sommerfeld radiation condition, coefficients  $a_0 = 1.04$ ,  $a_1 = 0.106$  and  $b_1 = 0.289$ , taken from Luppès et al. [2010], fig. 8.

This expression is used in the development of the active boundary condition implemented in IHFoam, as it will be shown in 3.0.2.

## 2.3 Previous works

Numerous publications exist that try to analyse or reproduce the loads on a long cylinder exposed to a oscillatory flow. From the classical papers of [Stokes \[1851\]](#),[\[Wang, 1968\]](#), [\[Honji, 1981\]](#) or [\[Hall, 1984\]](#), to experimental papers of [Sarpkaya \[1986\]](#), [Otter \[1990\]](#) or [Chaplin \[2000\]](#) among many others.

Apart from the aforementioned, there have been some other recent relevant studies more specifically related to the scope of this project:

1. [Schäffer and Klopman \[2000\]](#) develops an active absorption boundary condition based on digital filtering tailored for shallow water conditions, which is the base for IHFoam tool.
2. [Afshar \[2010\]](#) built a numerical wave tank with tailored boundary conditions to generate a 5<sup>th</sup> order Stokes wave, using relaxation zones for generation and absorption, measuring 1 wave length for generation and 3 for absorption zones, and focussed on the calculation of the error with theoretical solution, but was unable to validate his wave tank against experimental results.
3. ComFLOW® is another numerical model developed by [Luppés et al. \[2010\]](#) for numerical wave tanks, this model uses the cutting cell method, which is said to have less computational cost but also to be less robust compared to the adaptative meshing method of OpenFOAM® [Higuera et al. \[2013\]](#).
4. [Paulsen et al. \[2012\]](#) used InterFoam solver together with *waves2foam* boundary condition toolbox, one of the passive absorption type, to successfully model loads on submerged cylinders mainly in shallow and intermediate water depth conditions, validated against the measurements from [Huseby and Grue \[2000\]](#).
5. [Higuera et al. \[2013\]](#) included a thorough description of the IHFoam approach and generation and absorption boundary conditions, including validation of two dimensional and three dimensional cases, with solitary and cnoidal waves in shallow water. A series of papers related to coastal applications and porous structures came later on.
6. [Peng \[2014\]](#) used *waves2foam* approach –passive absorption – to model slamming forces on breaking waves on cylinders, validating them against the experiments from [Ting and Kirby \[1994\]](#).

No work has been done to date that tries to assess the application of IHFoam environment to the simulation of wave loading on cylinders.

## Chapter 3

# Numerical Model Description

The tool used to model the cases presented in chapter 5 were run within OpenFOAM® environment, version 2.2.2, using InterFoam solver and IHFoam routines.

OpenFOAM® is a free, open source CFD software package developed by OpenCFD Ltd at ESI Group and distributed by the OpenFOAM® Foundation. The OpenFOAM® environment includes a sets of solvers for different physical problems, with focus on fluids, and a number boundary conditions that is growing continuously with the support of the open source community. It is widely used by the research international community and its solvers have been extensively validated in numerous publications in the recent years. More details about the model can be obtained in [Weller et al. \[1998\]](#) and <http://www.openfoam.org/>.

The package comes with independent C++ libraries tailored for specific condition and assumptions based on the RANS equations (incompressible, supersonic, multiphase, potential ...), and a set of boundary conditions to solve those, which is constantly growing (Dirichlet, Neumann (gradients), and combined boundary conditions).

InterFoam is a multiphase solver for incompressible fluids that uses a Volume of Fluid (VOF) method within OpenFOAM®, a rather simple technique to solve the complex interaction of the phases at the interface (or *free surface*), see section 2.2.1.

IHFoam is a tool developed by the Hydraulic Institute of Cantabria (Spain) that needs to be compiled within InterFOAM, a two phase solver from the OpenFOAM® family for incompressible flows. The version currently used for this project is IHFoam 2.0. An overview of the model can be obtained at <https://openfoamwiki.net/index.php/Contrib/IHFOAM>

### 3.0.1 Equations

The governing equation of the specific solver InterFoam – used for all the simulations included in this document – are the RANS equations for incompressible fluids, including the VOF approach for a 2 phase flow, as mentioned in section 2.2.1.

### 3.0.2 Boundary Conditions

Boundary conditions in OpenFOAM® can be either of a *base type* or *numerical type*. *Base type* is a type of patch described purely in terms of geometry or a data communication link (*symmetryPlane* or *empty* boundary conditions). *Numerical type* assigns the value to the field variables in the given patch. The latter can be of primitive type – the base numerical patch condition assigned to a field variable on the patch – or derived type – a complex patch condition, derived from the primitive type, assigned to a field variable on the patch. Mathematically speaking, the *numerical type* can be either Dirichlet,



Neumann or Robin type.

Since the model is for incompressible fluids and laminar flow, we only need to set boundary conditions for velocity, pressure and the VOF field values (*alpha field*).

Total pressure only needs to be specified at one boundary, usually the top boundary (atmosphere), setting it to zero value for convenience. The rest of the boundaries use *buoyantPressure* that sets a *fixed-Gradient* pressure –specifying a gradient for P normal to the boundary – based on the atmospheric pressure gradient .

Here is a brief explanation of other boundary conditions used in this project:

1. *fixedValue*: the value of a variable (vectorial or scalar) is specified at the boundary.
2. *empty*: Since OpenFOAM®always generates geometries in three dimensions, this boundary condition instructs the software to solve in 2D, leaving the dimension normal to the plane of the boundary as a dummy dimension. This is the case for the front and back walls in the 2D simulations.
3. *zeroGradient*: Gradient normal to the patch is set to zero –i.e. extrapolates values from the domain. Only applicable to scalar variables.
4. *symmetryPlane*: Applies to planar faces where symmetry exist in the geometry and the flow field for the three dimensional simulations. Used for the plane of symmetry containing the axis of the cylinder and a vector in the x direction. It implies:
  - Zero normal velocity at the symmetry plane.
  - Zero normal gradients of all variables at symmetry plane.
5. *slip*: *zeroGradient* if applied to a scalar; if applied to a vector, normal component is set to zero, tangential components are set to *zeroGradient*.
6. *inletOutlet*: Switches U and p between *fixedValue* and *zeroGradient* depending on direction of U.
7. *pressureInletOutletVelocity*: Combination of *pressureInletVelocity* –When p is known at inlet, U is evaluated from the flux normal to the patch– and *inletOutlet*.

## Wave generation

The wave generation boundary condition is the starting point of the model. An accurate generation of incident waves is of utmost importance to get aimed wave forms and velocities through out the domain and avoid noise, spurious waves and currents. For instance, breaking waves are very sensitive to wave profiles, any anomalies introduced in the wave can cause rising of non linearities and early breaking.

Trying to use the *setFields* utility from OpenFOAM®to impose inlet boundary conditions is a very rough way of including values for the alpha field or for the velocities, very inaccurate for our purpose, since it only considers either wet ( $\alpha = 1$ ) or dry cells ( $\alpha = 0$ ), but nothing in between.

There are a couple of relevant attempts available in the literature to implement a time dependent boundary condition for the interphase level within InterFoam [Higuera et al., 2013]:

- Using GroovyBC, an opensource boundary condition that allows to impose any mathematical expression for the water phase level with time. It needs an explicit approximation of the free surface, needing an analytic calculation of the wavelength, so it is only suitable for Stokes I and II theories.
- Some other authors, like Jacobsen et al. [2012], have proposed a complete solution to this, accounting for wet, dry and partially filled cells. This solution applies only to passive absorption boundaries, by means of relaxation zones, not being applicable to IHFoam.

IHFoam doesn't use any of the above, it includes a tailored module, coded from scratch, to generate Stokes theory (I, II and V orders), cnoidal and stream function theories, Boussinesq and solitary waves. It also supports irregular waves based on linear and second order harmonics. All theories share the numerical implementation of the wave generation process.

Only free surface, through the VOF function values ( $\alpha_1$  field or  $\alpha_1$ ) and velocities are specified at the inlet patch (an open boundary in OpenFOAM®), since imposing pressure would lead to an over specified problem.

The numerical scheme considers for every time step the theoretical and the measured water level at the inlet patch, in order to consider the effects of high amplitude reflected waves arriving to the inlet. For this matter, three zones are established depending on the elevation ( $z$  coordinate) at the generation patch in order to define the boundary conditions for  $U$  and  $\alpha_1$  (see fig. 3.1):

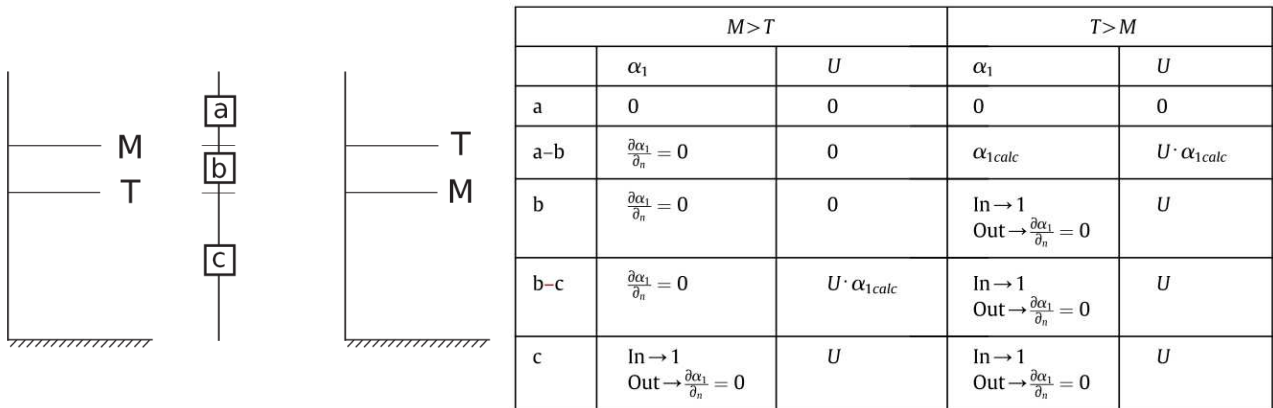


Figure 3.1: Three areas (a,b,c) in which the inlet patch is divided to define the boundary conditions for  $U$  and  $\alpha_1$  (left) and a table that summarizes the definition of the boundary conditions (right), extracted from Higuera et al. [2013].  $M$  stands for measured value,  $T$  for theoretical value.

Boundary conditions are set depending on the case:

- Zone a: Air phase, the faces of the boundaries have velocities and  $\alpha_1$  set to zero.
- Interface of zones a-b: If  $M > T$  a zero gradient condition for  $\alpha_1$  and zero value for  $U$ . If  $M < T$  the theoretical water level is intersected with the mesh at the patch to obtain  $\alpha_1$  value of the cell, the centroid of this cell is obtained to calculate the velocity at that point using the theory  $U$ , the imposed velocity is the multiplication of those values  $U \cdot \alpha_1$ . This is done to avoid spurious high air velocities at the boundary that would lead to instabilities and lower the required Courant

number and time step.

- Zone b: If  $M > T$  we have the same conditions as before. If  $M < T$   $\alpha_1$  is set to one if the flow is entering the domain and to zero gradient otherwise, velocities are set to values according to theory.
- Interface of zones b-c: If  $M > T$   $\alpha_1$  is set to zero gradient and velocity is calculated following the procedure described for interface a-b. If  $M < T$   $\alpha_1$  is set to one if the flow is entering the domain and zero gradient otherwise.  $U$  is set to the theoretical value.
- Zone c: filled with water,  $U$  is set to the corresponding theoretical value,  $\alpha_1$  is set to one if the flow is entering the domain and zero gradient otherwise. This is said to be more stable and avoids  $\alpha_1$  from reaching negative values.

### Active wave absorption

The active wave absorption boundary condition implemented in IHFoam is meant to work alone or together with wave generation. This, in theory, allows for longer simulations without linear reflections. It is based on the superposition principle by generating a velocity field  $U_c$  in the opposite direction to that of the reflected wave to cancel the reflection.

The boundary conditions is based on the work by [Schäffer and Klopman \[2000\]](#), considering linear shallow water theory, where a constant velocity profile  $U$  can be assumed, that is related to the wave celerity  $c$  by means of eq. 3.1 the given expression:

$$Ud = c\eta \quad (3.1)$$

Following the thread from section 2.2.4, the difficult point here is the calculation of  $c$  to include a wide range of harmonics in eq. 2.40, but if we consider shallow water theory, the dispersion relation can be simplified to  $c = \sqrt{gd}$  for every harmonic no matter the frequency, which is very convenient. This leads us to the expression in eq. 3.2.

$$U_c = -\sqrt{\frac{g}{h}}\eta_r \quad (3.2)$$

Where  $U_c$  is the correction velocity perpendicular to the boundary pointing into the domain, and  $\eta_r$  is the amplitude of the linear reflected wave, which can be estimated by measuring the level at the wavemaker (inlet patch)  $\eta_m$ , and subtracting the target elevation  $\eta_t$  (from the Fenton solution), according to the one expected as if no reflections would occur.

$$\eta_r = \eta_m - \eta_t \quad (3.3)$$

# Chapter 4

## Methodology

In this chapter we will describe the procedure to get the results presented in chapter 5.

All the simulations in this project were run within OpenFOAM® version 2.2.2 environment, using InterFoam VOF solver and IHFoam routines: i) *IH\_Waves\_InletAlpha* and *IH\_Waves\_InletVelocity* generation for  $\alpha$  and velocity (U) fields, and active absorption boundary conditions for the U fields at the inlet patch; and ii) *IH\_3D\_2DAbsorption\_InletVelocity* for the active absorption for U and the outlet patch. This latter is preferred to the three dimensional tailored boundary condition *IH\_3D\_3DAbsorption\_InletVelocity* when the incoming waves are perpendicular to the patch surface [Higuera et al., 2013], which is assumed to be consistent for all the cases, even for the three dimensional simulations, since in those cases the reflections with the cylinder are negligible compared to the target waves.

The two dimensional simulations were all set within a linux environment, using a laptop with 4 cores, 7.5 GiB of RAM and 4 processors Intel® Core™ i3-2375M CPU @ 1.50GHz.

The three dimensional simulations have been run in a unix cluster, with a variable number of nodes involved in each simulation, in a case to case basis. The general rule was to involve around 100.000 cells per node.

All simulations have used a dynamic time step setting, with a maximum Courant number of 0.5 to ensure stability and convergence.

### 4.1 Two dimensional simulations

These simulations were picked from the literature in order to assess the performance of the tool for a given range of conditions, mainly with varying depth to length ratio and steepness  $\epsilon = \frac{H}{L}$ , as a previous phase for modelling more complex three dimensional cases.

The table 4.1 shows a list of the simulations considered with some relevant dimensionless parameters. For each of those, a two dimensional domain has been designed according to dimensions provided in Paulsen et al. [2012]. This domain is sketched in figure 4.2.

Paulsen et al. [2012] cases are taken from the three dimensional simulations included in table 1 in that paper. The simulations are done using *waves2foam* tool, also based in InterFOAM but using relaxation zones. The stream function for the 2D validation of the generation model in that same publication is also included among the simulations (H=10 m, T=14 s, d=20 m). Moreover, since this case has behaved reasonably well in the model, an extension of these cases have been used to assess

---

<sup>1</sup>Summary of simulations considered in this work

Source	N <sup>1</sup>	Wave theory	H/L	d/L
<a href="#">Paulsen et al. [2012]</a> table 1	6	stream function	0.042-0.092	0.082-0.247
<a href="#">Paulsen et al. [2012]</a> two dimensional validation (inc. extension)	11	stream function	0.033-0.05	0.1-2.29
OC5 tests	6	Stokes 5 <sup>th</sup>	0.041-0.082	1.360-2.671
<a href="#">Grue and Huseby [2002]</a> tests	2	stream function	0.089/0.093	0.486/0.721

Table 4.1: *Data sets considered for two dimensional simulations*

the performance of the model for deeper waters ( $d=20, 30, 40, 50, 60, 80, 120, 155, 190, 700$  m).

One more simulation, also derived from the two dimensional validation case used in [Paulsen et al. \[2012\]](#), was included as an extension to have a case well within the limits of the model (low steepness and shallow water), ( $H=8$  m,  $T=14$  s,  $d=20$  m). This case has also been included in the three dimensional simulations.

OC5 cases are a set of small scale experiments made in the Phase I of the OC5 Program referred to Offshore Wind Systems, that took place in MARINTEK wave flume in Trondheim, in order to validate code results to physical test data. The flume is in a 80 m long tank, 10.5 m wide, and 10 m deep, equipped with a hydraulic double-flap long crested wavemaker at one end.

[Grue and Huseby \[2002\]](#) tests were carried out in a tank that was 24.57 m long, 0.5 m wide and a water depth of 0.6 m, with a piston type wavemaker.

In figure 4.1, an graphical overview of all the two dimensional simulations is presented, together with the applicability of the different theories. Most of the waves are in the intermediate depth range. Note also that the stream function wave can be applied anywhere in the stability range of waves, as discussed in 2.1.3, and has been used widely in the literature gathered as the base for this present work.

#### 4.1.1 Domain

The length of the domain has been chosen to be at least as long as the wave length, but in the cases from the OC5 project, the length has been chosen to be twice that value, in order to avoid having the reflective outlet patch too close.

The height of the domain has been chosen as  $d + 2H$ , this has proven to be sufficient since no water has been found to overtake that limit.

The mesh resolution is usually determined by the *ppwh* –points per wave height – and is usually set around 10-15, since finer meshes will not lead to a perceptible improvement in the results [[Paulsen et al., 2012](#)]. The cell aspect ratio is set to 2, where  $\Delta x = 2\Delta z$ , where  $z$  is the axis in the vertical direction, and  $x$  is the axis in the direction of the wave propagation.

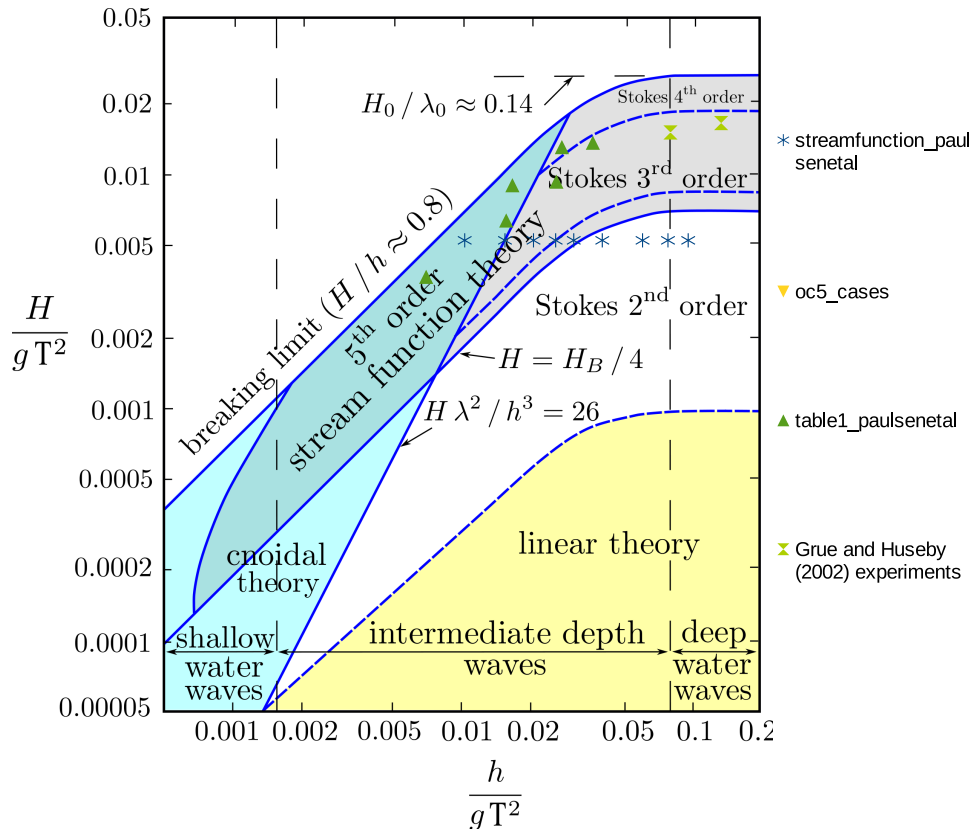


Figure 4.1: Summary of 2D cases together with suitable wave theories, taken from Méhauté [1976].  $H$  is the wave height,  $h$  is the water depth,  $\lambda$  is the wave length and  $T$  is the wave period

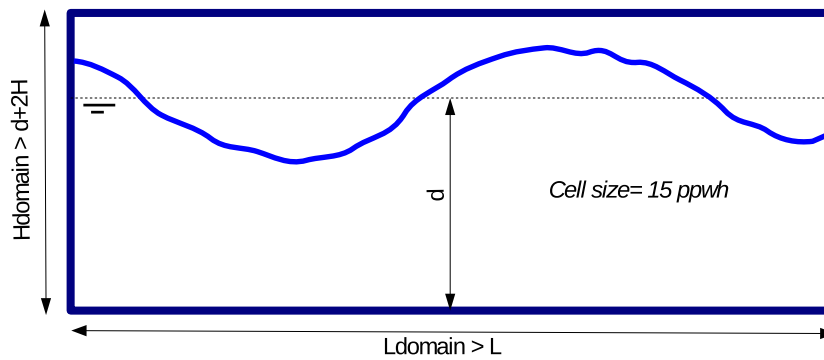


Figure 4.2: Domain for two dimensional simulations,  $L$  is the wave length,  $H$  is the wave height and ppwh stands for points per wave height

### 4.1.2 Boundary Conditions

The boundary conditions used for pressure, alpha and velocity fields, within the two dimensional simulations are summarized in table 4.2.

### 4.1.3 Diffusive error

The performance of IHFoam to simulate and propagate the waves is validated against theory. Stream function theory [Fenton and Rienecker, 1982] is used for Paulsen et al. [2012] and Grue and Huseby

<sup>1</sup>Number of cases considered

Boundary	P	$\alpha$ field	U
Inlet	<i>buoyantPressure</i>	<i>IH_Waves_InletAlpha</i>	<i>IH_Waves_InletVelocity</i>
Outlet	<i>buoyantPressure</i>	<i>inletOutlet</i>	<i>IH_3D_2DAbsorption_InletVelocity</i>
Top	<i>totalPressure(0)</i>	<i>zeroGradient</i>	<i>pressureInletOutletVelocity</i>
Bottom	<i>buoyantPressure</i>	<i>zeroGradient</i>	<i>slip</i>
FrontandBack	<i>empty</i>	<i>empty</i>	<i>empty</i>

Table 4.2: *Boundary conditions for two dimensional simulations*

[2002] cases and Stokes 5<sup>th</sup> theory is used for validation of OC5 cases.

An estimation of the error in the two dimensional simulations have been included in order to quantify this performance against theory. This error is defined as:

$$\epsilon_d = \frac{1}{H} \sqrt{\sum_{i=1}^{N_T} \frac{(\eta_i^{foam} - \eta_i^{th})^2}{N_T}} \quad (4.1)$$

Where  $N_T$  is the number of points within a wave period  $T$ ,  $\eta^{foam}$  is the free surface elevation from the still water surface as obtained from IHFoam model,  $\eta^{th}$  is the same elevation as obtained from the theoretical solution, which has been obtained by means of the software tool created by Fenton [2014] and freely available through his web page. This tool provides a numerical solution for the two non linear theories used in this project: stream function theory [Fenton and Rienecker, 1982], and Stokes 5<sup>th</sup> theory.

The diffusive error is measured in a gauge situated at the middle of the flume for a whole wave period duration and for 4 different wave periods, from the 5<sup>th</sup> to the 8<sup>th</sup> wave, starting at the moment when the wave actually reaches the gauge. This will give us an idea of the performance of the model and the existence of numerical diffusion.

The theoretical solution is shifted to match the zero upcrossings in both plots for the 5<sup>th</sup> wave of the record, and later refining the shift of the theoretical solution in order to minimise the error as defined in 4.1.

#### 4.1.4 Reflection coefficient

In order to assess the performance of the active absorption boundary condition included in IHFoam software tool, as described in 3.0.2, a quantification of the reflections is needed. This has been done following the procedure described in Goda and Suzuki [2011].

The method uses the Fourier series approximation of the time series of the free surface elevation  $\eta$  at two gauges, with a separation between them  $\Delta l$  that has to fulfil that is not a multiple of half the wave length :  $\Delta l \neq \frac{nL}{2}$ , where  $n = 0, 1, 2, \dots$ . This is to avoid a divergence in the calculation of the reflection coefficient, that is  $\sin(k\Delta l) = 0$ , giving  $R \rightarrow \infty$ .

As a general rule, the two gauges were located at the midflume, with a separation of  $\Delta l = \frac{L}{9}$ . The reflection coefficient is obtained by approximating a Fourier series of the surface elevation of the two gauges  $j = 1, 2$ :

$$\eta_j = \sum_{i=1}^N A_{ji} \cos(\omega_i t) + B_{ji} \sin(\omega_i t) \quad (4.2)$$

Where  $A_{ji}$  and  $\omega_i$  are the amplitude and the angular frequency of the  $i^{\text{th}}$  harmonic at gauge  $j$ .

The reflected and incident wave amplitudes  $A_i$  and  $A_r$  can then be approximated for a monochromatic wave as:

$$A_i = \frac{1}{2|\sin(k\Delta l)|} \sqrt{(A_2 - A_1 \cos(k\Delta l) - B_1 \sin(k\Delta l))^2 + (B_2 + A_1 \sin(k\Delta l) - B_1 \cos(k\Delta l))^2} \quad (4.3)$$

$$A_r = \frac{1}{2|\sin(k\Delta l)|} \sqrt{(A_2 - A_1 \cos(k\Delta l) + B_1 \sin(k\Delta l))^2 + (B_2 - A_1 \sin(k\Delta l) - B_1 \cos(k\Delta l))^2} \quad (4.4)$$

This equation can also be applied to each harmonic independently by means of the superposition principle, so to obtain the reflection coefficient for each harmonic frequency. The reflection coefficient is, in reality, dependent on the frequency  $r = f(\omega)$ . In this project, the reflection coefficient for both the fundamental frequency and the second harmonic have been obtained, and also a weighted average of the whole spectral resolution (see [Goda and Suzuki \[2011\]](#)) with the square of the incident amplitude, that average gives us an idea of the reflection coefficient in terms of energy.

From the incident and reflected amplitudes  $A_i$  and  $A_r$ , the incident and reflected spectrum  $S(f)$  can be obtained by eq. 4.5 for every frequency bandwidth  $\Delta f$  for the  $j^{\text{th}}$  harmonic.

$$S(j \cdot \Delta f) = \frac{A(j \cdot \Delta f)^2}{2\Delta f} \quad (4.5)$$

It is important to remark that the procedure used to obtain the reflections –reflection coefficient and reflected spectra – is based on the superposition principle using the linear theory for all the harmonics in the wave, assuming the reflected energy is contained in the same frequency as the incident energy. Therefore, this method doesn't take into account non linear effects happening at the boundaries, such as breaking waves (total or partial) splashes, runups, ... which do happen in some of the simulations. It is, anyway, a good estimation of the performance of the boundary condition considering linear effects, for smooth waves. As far as the author is concerned, an alternative doesn't exist for accounting non linear effects in the computation of the reflection coefficient. This is a wide topic out of the scope of this Master Thesis, further work needs to be developed to assess the effect of non linearities on reflections at the boundaries.

## 4.2 Three dimensional simulations

The three dimensional cases are picked from the literature, and they are also included among the two dimensional set. It is thought that way in order to first assess the wave generation and boundary conditions and then the pressure forces.

A summary of the cases, together with the relevant parameters of the waves and cylinder diameter  $D$  is shown in table 4.3.

---

<sup>2</sup>Number of simulations considered



Source	$N^2$	Wave theory	H/L	d/L	D[m]	$N_{KC}$
Paulsen et al. [2012] table 1	4	stream function	0.042-0.092	0.082-0.247	6	7.62-9.98
Paulsen et al. [2012] two dimensional validation	1	stream function	0.033-0.05	0.1-2.29	6	8.54-10.45
Grue and Huseby [2002] tests	2	stream function	0.089/0.093	0.486/0.721	0.06	10.73/7.56

Table 4.3: Data sets considered for three dimensional simulations

#### 4.2.1 Domain

The three dimensional cases are meant to obtain the loads on the vertical cylinders, the domain now is prismatic with similar dimensions than those of the two dimensional cases, these are shown in table 4.3.

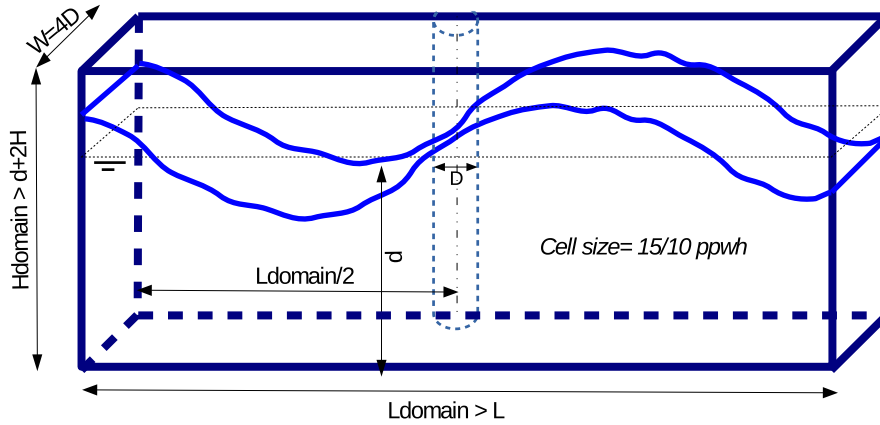


Figure 4.3: Domain for three dimensional simulations,  $L$  is the wave length,  $H$  is the wave height and ppwh stands for points per wave height

The mesh is uniform and rectangular with a cell size of 15 ppwh and a length of the domain of  $2L$  for all the cases except the OC5 project set, where the resolution is set to 10 ppwh and the length of the domain equal to  $L$ . This was necessary for keeping an affordable size for the model, since the OC5 cases are in very deep water compared to the wave height– 10 m versus 0.60 m.

The aspect ratio here is set to 1, so  $\Delta x = \Delta y = \Delta z$ .

#### 4.2.2 Boundary Conditions

The boundary conditions in space for the three dimensional cases, are summarized in table 4.4.

Boundary	P	$\alpha$ field	U
Inlet	<i>buoyantPressure</i>	<i>IH_Waves_InletAlpha</i>	<i>IH_Waves_InletVelocity</i>
Outlet	<i>buoyantPressure</i>	<i>zeroGradient</i>	<i>IH_3D_2DAbsorption_InletVelocity</i>
Top	<i>totalPressure(0)</i>	<i>inletOutlet</i>	<i>pressureInletOutletVelocity</i>
Bottom	<i>buoyantPressure</i>	<i>zeroGradient</i>	<i>slip</i>
Frontwall	<i>buoyantPressure</i>	<i>zeroGradient</i>	<i>slip</i>
symmetryplane	<i>symmetryPlane</i>	<i>symmetryPlane</i>	<i>symmetryPlane</i>
cylinder	<i>buoyantPressure</i>	<i>zeroGradient</i>	<i>slip</i>

Table 4.4: *Boundary conditions for three dimensional simulations*

# Chapter 5

## Results

### 5.1 Two dimensional simulations

In this section the relevant results will be presented for the two dimensional simulations, splitting them into wave generation, wave form and velocities.

#### 5.1.1 Wave Generation

The wave generation is done according to section 3.0.2. It has been found that wave generation is more accurate on smooth waves than on steep ones.

Following is a set of plots showing the relevant differences found among the cases considered mainly depending on the steepness  $H/L$ .

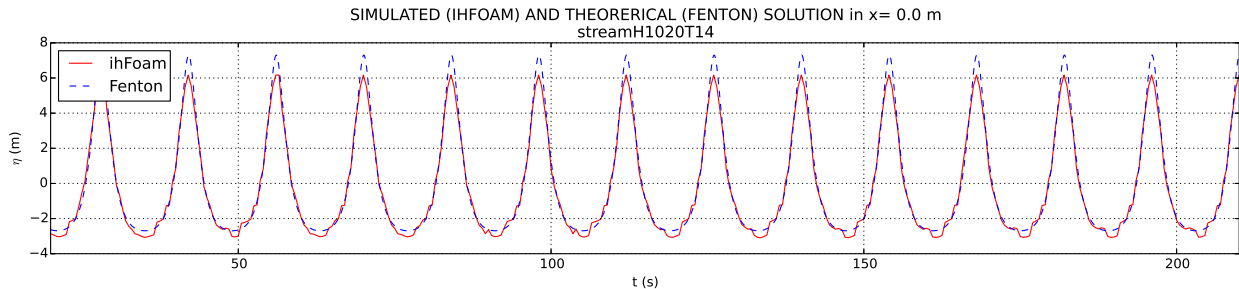


Figure 5.1: Generated water elevations at inlet patch,  $H/L = 0.05$  for a stream function wave. Estimated averaged error on generation of waves 5, 5+1, 5+2 and 5+3 is  $\epsilon = 0.047$ .

A general overview of those plots show how the wave generation performs well on steepness  $H/L < 0.05$  (figure 5.2 ) with crests 1 m lower than expected (10% error), but fails to accurately represent theory especially on steeper crests, see fig. 5.3 and 5.1 for an illustration on this. A non smooth staircase profile is observed on most cases, which can lead to noise in the tank. Afshar [2010] also observed this phenomena, but for a different wave generation numerical procedure. A finer grid is proposed by the aforementioned author to avoid this problem, despite of the higher computational cost.

A more refined mesh has been essayed to further investigate this issue following the reasoning by Afshar [2010]. Nevertheless, refining the mesh to half the size of the initial mesh size –i.e. from 15 to 30 ppwh– did not produce any improvement, in fact, the error in the generated wave form increases if the mesh is refined, see 5.4.

Certain improvement to this generation error is achieved though, if we remove the compression term from eq. 2.34, by setting  $cAlpha$  coefficient to 0. The result on the same case as in 5.3 is shown in

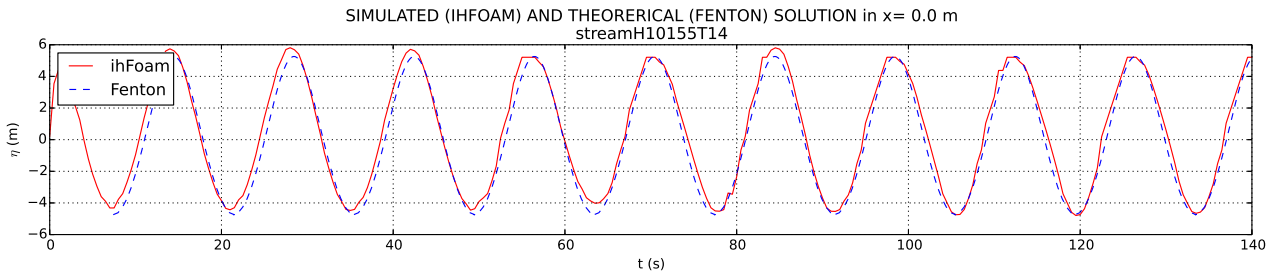


Figure 5.2: Generated water elevations at inlet patch,  $H/L = 0.032$ , for a stream function wave. Estimated averaged error on generation of waves 5, 5+1, 5+2 and 5+3 is  $\epsilon = 0.057$ .

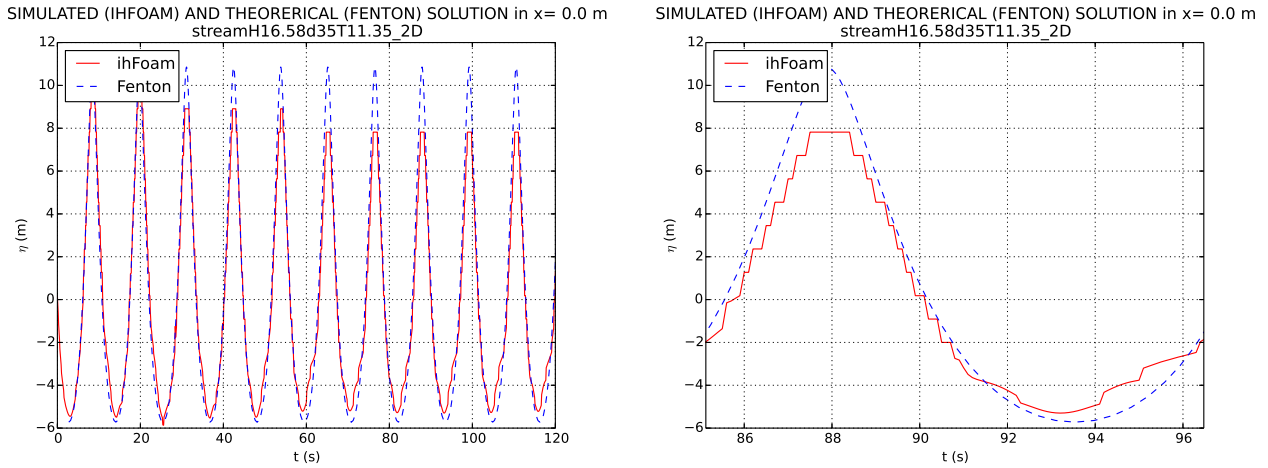


Figure 5.3: Generated water elevations at inlet patch,  $H/L = 0.092$ , for a stream function wave. A staircase profile can be observed in the wave form. Estimated averaged error on generation of waves 5, 5+1, 5+2 and 5+3 is  $\epsilon = 0.071$ .

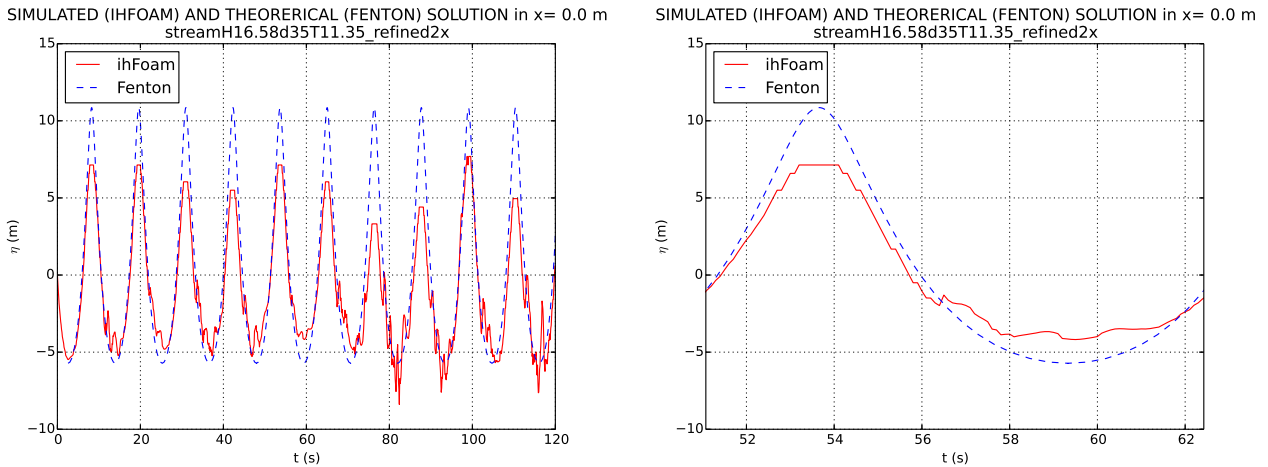


Figure 5.4: Generated water elevations at inlet patch, same case as fig. 5.3, but an aspect ratio  $\Delta x/\Delta z = 1$  and 30 ppwh. Estimated averaged error on generation of waves 5, 5+1, 5+2 and 5+3 is  $\epsilon = 0.143$ .

fig. 5.5.

This staircase profile fades when giving enough space for the wave to "settle", but spurious effects can be induced in the wave and the velocities, which may contribute to the observed non linearities in section 5.1.2.

In table 5.1, the average error in the wave generation  $\hat{\epsilon}_0$ , together with this same error in the

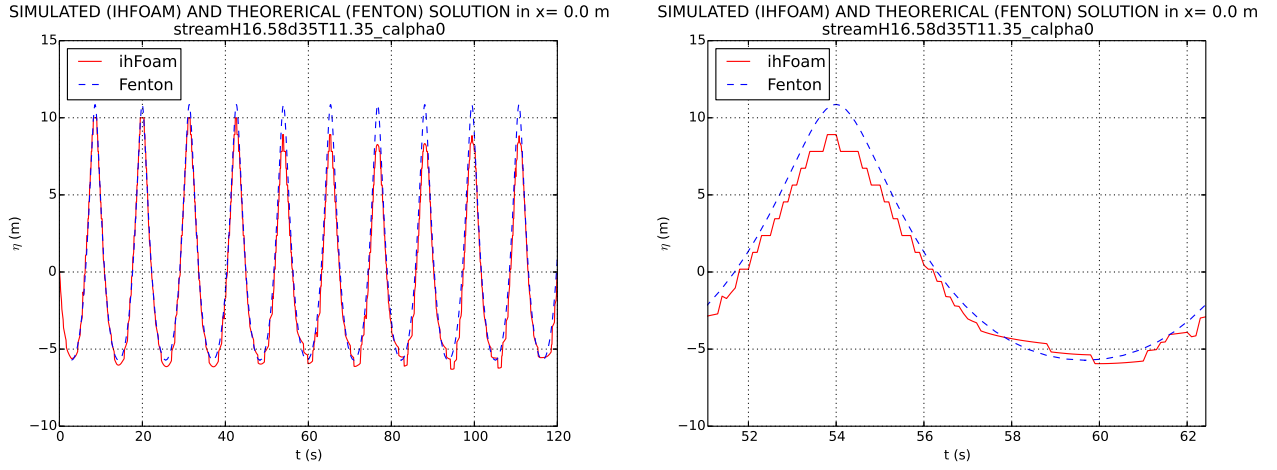


Figure 5.5: Generated water elevations at inlet patch, same case as fig. 5.3, but compression ratio coefficient  $cAlpha$  is set to 0. Estimated averaged error on generation of waves 5, 5+1, 5+2 and 5+3 is  $\varepsilon = 0.062$ , an improvement of -1.4% in the error.

midflume  $\hat{\varepsilon}_m$ , is presented for the stream function theory among four cases included in table 1 within Paulsen et al. [2012]. There seems to be a direct relation between the steepness  $H/L$  and the error in the generation. On the other hand, removing the compression term improves the generation error in about 1% (not in every case though) and seems to lead to a higher error at the midflume.

Source	cAlpha	H [m]	T[s]	d[m]	H/L	$\hat{\varepsilon}_0$	$\hat{\varepsilon}_m$
Paulsen et al. [2012] table 1-case 2	1	10.02	12.7	25	0.055	0.056	0.069
Paulsen et al. [2012] table 1-case 2	0	10.02	12.7	25	0.055	0.049	0.115
Paulsen et al. [2012] table 1-case 4	1	12.44	11.67	35	0.068	0.054	0.063
Paulsen et al. [2012] table 1-case 4	0	12.44	11.67	35	0.068	0.026	0.092
Paulsen et al. [2012] table 1-case 20	1	13.36	12.31	25	0.074	0.068	0.072
Paulsen et al. [2012] table 1-case 20	0	13.36	12.31	25	0.074	0.064	0.080
Paulsen et al. [2012] table 1-case 22	1	16.58	11.35	35	0.092	0.071	0.089
Paulsen et al. [2012] table 1-case 22	0	16.58	11.35	35	0.092	0.062	0.064
Paulsen et al. [2012] table 1-case 12	1	10.86	8.99	30	0.090	0.100	0.069
Paulsen et al. [2012] table 1-case 12	0	10.86	8.99	30	0.090	0.099	0.109

Table 5.1: Summary of errors in wave generation ( $\hat{\varepsilon}_0$ ) and propagation at the midflume ( $\hat{\varepsilon}_m$ )

Plot in figure 5.6 summarizes the generation error of the selected cases from Paulsen et al. [2012],

table1.

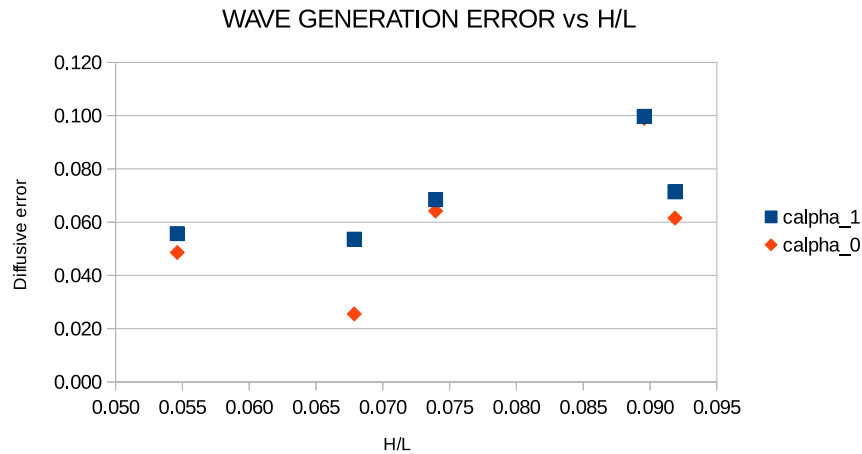


Figure 5.6: Wave generation error depending on the steepness switching the compression term on ( $cAlpha=1$ ) and off ( $cAlpha=0$ ).

### 5.1.2 Wave Propagation

The performance within the flume, specially at the midflume, where a potential structure would be located, is assessed in this section. A number of relevant simulations are presented, illustrating three different phenomena affecting the results:

- Wave skewness and early breaking: it is observed that, when including the numerical compression technique of the velocity as defined in 2.34, waves with steepness  $H/L > 0.05$  will develop skewness, breaking the symmetry of the wave form, and will break if given enough propagation length, see fig. 5.7. Removing this compression term completely –i.e.  $cAlpha$  factor set to 0 – solves the problem, maybe an intermediate solution could also be valid, further investigation is required to test the effects of this parameter in the solution. For the sake of this project, only values 0 and 1 have been included in the results.



Figure 5.7: Breaking wave, earlier than expected,  $H = 13.36m$ ,  $T = 12.31s$ ,  $d = 25m$ ,  $H/L = 0.074$  and  $H/H_{max} = 0.81$ , for a Stream function wave.

- Reflections coming from the inlet and outlet boundaries. Those can be either from linear or non linear reflections. The linear reflections can be quite limited well into the intermediate depth range, a reflection coefficient of less than 10% can be obtained for  $d/L < 0.16$ . The non linear

reflections are more difficult to predict and may appear on steep waves, in order to limit those, and based on the simulations included in this project, a steepness of  $H/L < 0.07$  could be a rough indication. This non linear reflections are more harmful if the waves are short ( $T$ ; 3-4 s), usual in scaled wave tank tests, since the splashes and other non linearities seem to create energy in that frequency range. This is the case of all the OC5 set, where  $d/L > 1.2$  and stationary resonant waves form due to the full reflection with the outlet and inlet. These have been removed from the results of the three dimensional simulations, since they show a very poor performance already in a simpler two dimensional setup.

On fig. 5.8 an extended case from the validation in Paulsen et al. [2012] is shown, modified to be in very deep water conditions, with a smooth wave form to limit the expected nonlinearities. This case seems to suffer mainly from linear reflections from the outlet, with the same frequency as the incident wave. If we compare this case with fig. 5.9, where the wave shows peaks, non linear reflections splashing and partial breaking, may introduce noise in a different frequency.

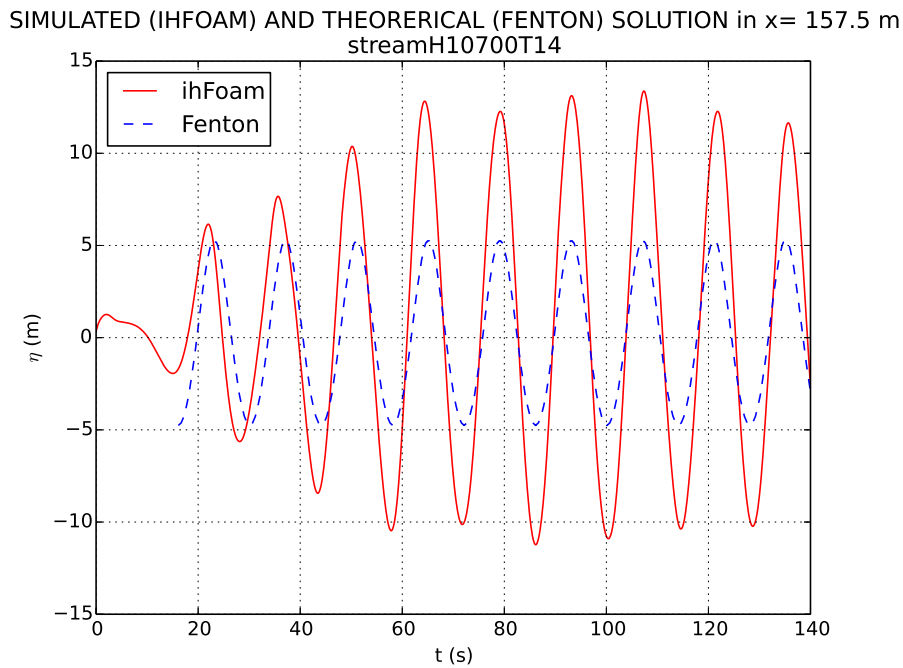


Figure 5.8: Simulation showing linear reflections,  $H = 10m$ ,  $T = 14s$ ,  $d = 700m$ .

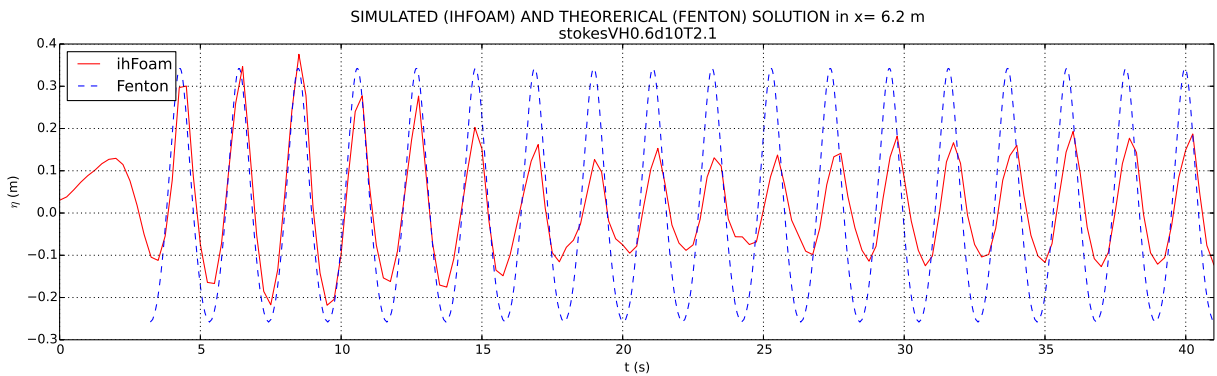


Figure 5.9: Simulation showing non linear reflections,  $H = 0.6m$ ,  $T = 2.1s$ ,  $d = 10m$ , from the OC5 case set.

On figure 5.11 and 5.12 a representative example of the OC5 case is presented, those cases are all in very deep water  $d/L > 1.3$ , well out of the range where the active absorption boundary condition is tailored. On the one hand, non linear reflections deteriorates the wave form after 10

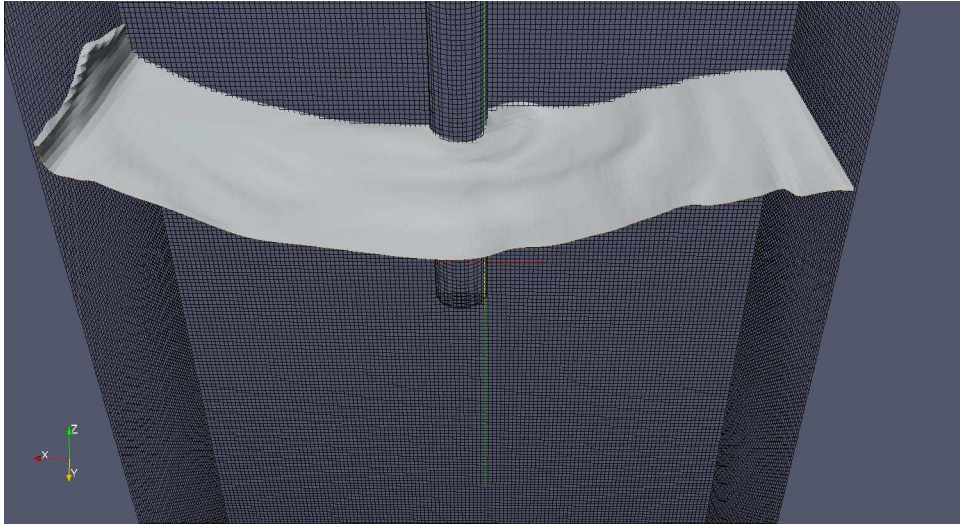


Figure 5.10: Simulation showing non linear interactions with the outlet,  $H = 0.28m$ ,  $T = 1.52s$ ,  $d = 10m$ , from the OC5 case set.

periods (5.11) including noise with different frequencies from the ones in the incident wave, on the other hand, the linear reflections create a stationary wave due to the high reflective boundaries (5.12).

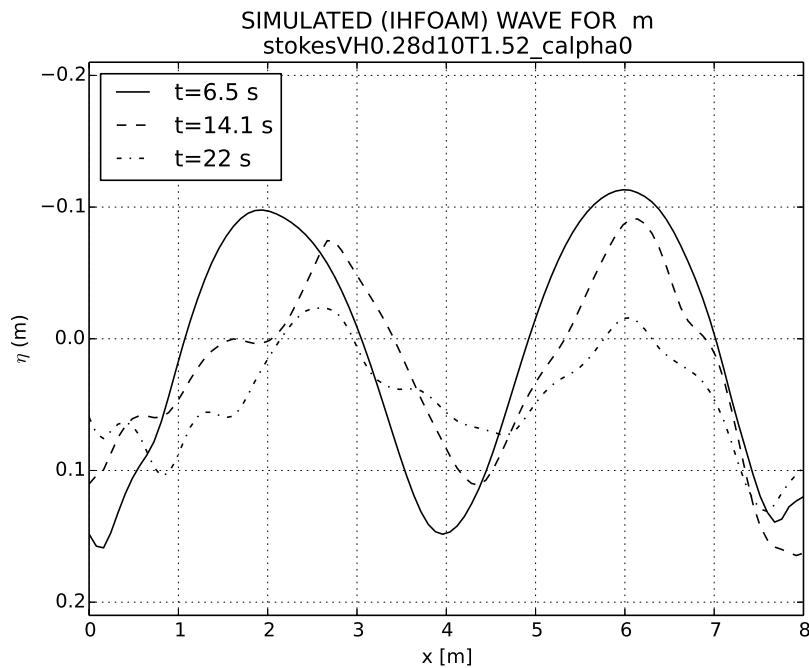


Figure 5.11: Simulation showing distortion of the wave form non linear reflections after 5, 10 and 15 periods,  $H = 0.28m$ ,  $T = 1.52s$ ,  $d = 10m$ , from the OC5 set.

The relation between the reflection coefficient, as defined in 4.1.4, and the relative wave depth is presented in figure 5.13, showing a direct relation between those.

- Spurious velocities coming from the wave absorption boundary condition: as has already been described in section 3.0.2, the active boundary condition is based on an artificial imposed velocity field that cancels the measured reflected wave from the outlet patch. It is based on shallow water theory so it is constant throughout the depth, but since this assumption is not fully met



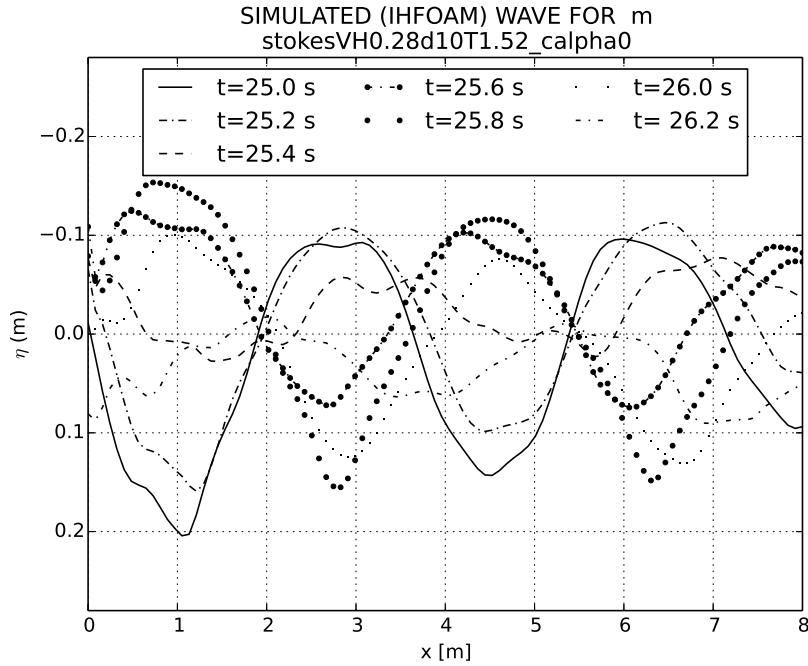


Figure 5.12: Simulation showing reflections causing stationary waves with 4 nodes (domain= $2L$ ),  $H = 0.28m$ ,  $T = 1.52s$ ,  $d = 10m$ , from the OC5 case.

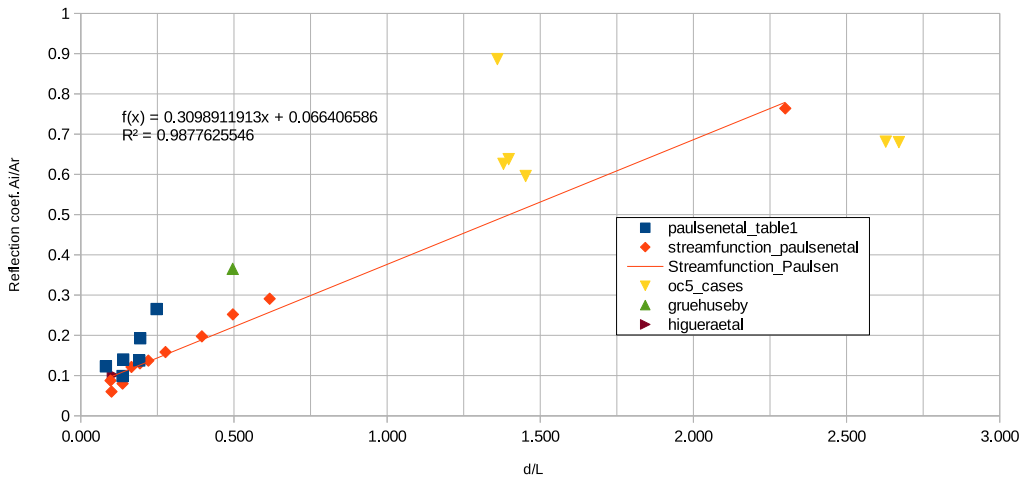


Figure 5.13: Plot of reflection coefficient on the first harmonic (fundamental frequency) against  $\frac{d}{L}$  showing a clear trend towards higher reflections in deeper waters.

on the cases presented, which are mostly within the intermediate water depth range, spurious currents are generated from the residuals of the cancelation velocity and propagated upwind towards the inlet, this could affect the wave stability. Of course this is more evident in very deep water, an example of this case with  $d/L = 2.287$  is shown in figure 5.14.

- Just as Afshar [2010] noted, spurious velocities, abnormally high, seem to be generated just above the surface in the air phase. According to this author, the cause of this might be that the VOF method solves one single transport equation for all the domain and only the densities make a difference when distributing scalar and vectorial properties between the phases of cells at the interface, and this is done by simple proportionality using the density as weighting func-

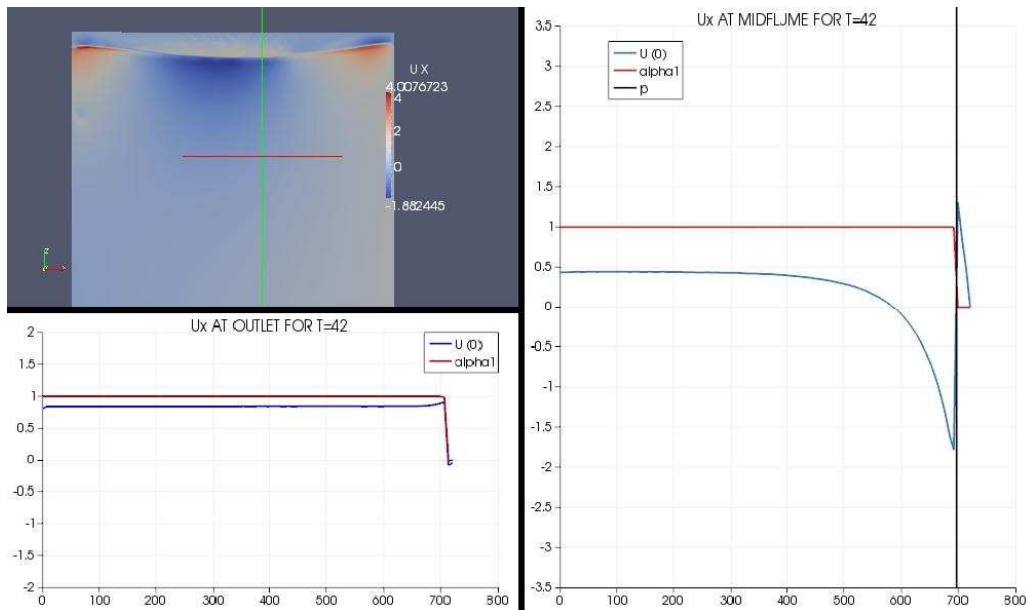


Figure 5.14: Spurious velocities in the water column (midflume, right plot), just over the bottom the horizontal velocities are opposite to the velocities of the wave (at the surface),  $H = 10\text{m}$ ,  $T = 14\text{s}$ ,  $d = 700\text{m}$ , for a Stream function wave.

tion, according to section 2.2.1. Partially filled cells share the momentum between the air phase and the water phase and, since the air has a density around 1000 times less than water, the gaseous phase gets unrealistic high velocities on the partially filled cells at the interface, that also drives the movement of the upper cells and creates an air current just above. This effect can be observed in fig. 5.15.

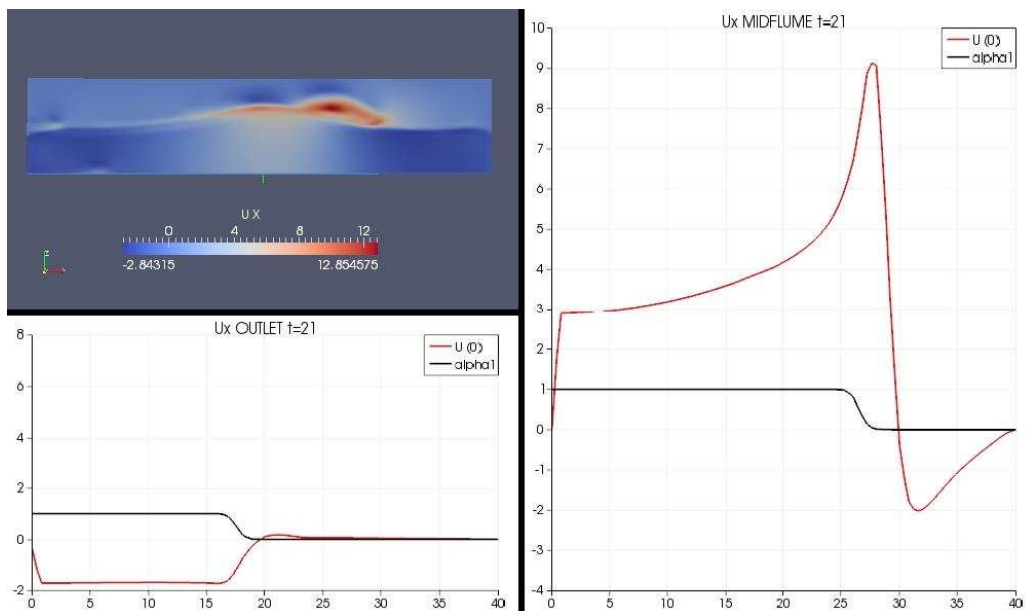


Figure 5.15: Artificially high air velocities just over the interface,  $H = 10\text{m}$ ,  $T = 14\text{s}$ ,  $d = 20\text{m}$ , for a Stream function wave. Velocities in [m/s].

- Spurious velocities coming from the outlet patch: The active wave absorption boundary condition includes cancelling velocities in the water filled cells, but also in the partially filled ones, giving momentum to the air phase, which is transmitted to the upper layers. This will create spurious air blows injected directly into the domain with high velocity see fig. 5.16 . That can

be an issue and affect the results if the air velocities are under study.

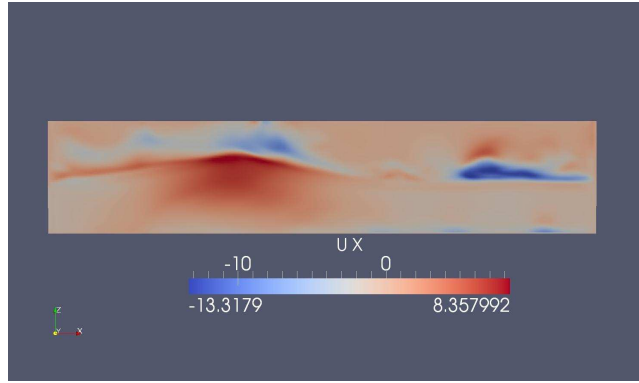


Figure 5.16: Spurious air velocities coming from the outlet (blows),  $H = 10m$ ,  $T = 14s$ ,  $d = 20m$ , Stream function wave. Velocities in [m/s].

Finally, a relation between the water depth and the measured error is presented in fig. 5.17. A trend can be observed showing a direct relation between those parameters. The correlation is not very high, since the error may depend on many other parameters, such as the wave steepness, the period or the Ursell number, to name a few.

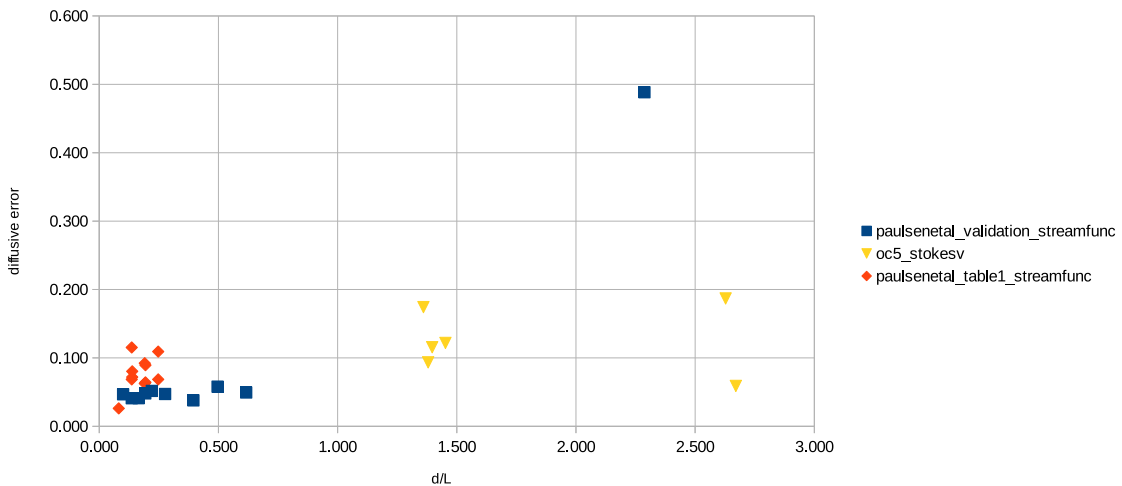


Figure 5.17: Plot of diffusive error (average value for 4 waves, as defined in 4.1.3) against  $\frac{d}{L}$

## 5.2 Three dimensional simulations

For completeness, a set of three dimensional simulations have been included in this project in order to obtain the forces on a simple structure – a vertical submerged cylinder. The cases considered have been obtained from the set used in the two dimensional simulations, picking only the ones in intermediate water depths from Paulsen et al. [2012] and Grue and Huseby [2002], since the OC5 cases, in very deep water conditions, have proven to be way out of the limit that restricts the good performance of the model. The selected cases, and its relevant parameters, are shown in table 4.3.

The forces are calculated by integration of the normal pressures around the cylinder by means of the *forces* function, integrated within *controlDict* dictionary. This is consistent with the fact that the cylinder patch is set to slip boundary condition to model an inertia dominated situation, considering

drag as negligible.

### 5.2.1 Simulations from Paulsen et al. [2012]

Figures 5.18 to 5.21 show the total inline force in Paulsen et al. [2012] cases divided in two different sets, depending on the value of  $H/H_{max} - H_{max}$  is defined in section 2.1.4. The results are compared with simulations from Paulsen et al. [2012] and with Morison forces, calculated from the velocities obtained from the Stream function theory. The simulations show that, without the compression term, the slamming forces are more obvious, since the waves tend to be steeper than theory. The results are obtained removing the compression term completely ( $cAlpha=0$ ), which show a better agreement with Paulsen et al. [2012] measurements and prevents early wave breaking.

The agreement with Paulsen et al. [2012] solution is quite good. A secondary load cycle appears on all simulations (even without the compression term), but it is more obvious when  $H/H_{max} > 0.6$ , while Paulsen et al. [2012] did not obtain them for  $H/H_{max} = 0.6$ .

The results are summarized in table 5.2, where the results with and without compression term ( $cAlpha=1$  and 0, respectively), can be compared. The loads are higher in the first case, specially in waves with steepness  $H/L > 0.07$  where the waves break over the cylinder (the other cases will break also, but at the end of the flume).

Source	H/L	cAlpha	Inline Force $\frac{F_{max}}{\rho g d D^2}$	
			Paulsen et al. [2012]	IHFoam
Paulsen et al. [2012] table 1- case 2	0.055	1	0.277	0.325
		0	0.277	0.273
Paulsen et al. [2012] table 1- case 4	0.068	1	0.253	0.293
		0	0.253	0.240
Paulsen et al. [2012] table 1- case 20	0.074	1	0.461	0.736
		0	0.461	0.469
Paulsen et al. [2012] table 1- case 22	0.092	1	0.450	0.683
		0	0.450	0.414

Table 5.2: Summary of results for the total inline forces in the cylinder together with the compared values from other sources. The IHFoam results are an average of all the waves within the simulation time.

### 5.2.2 Experiments from Grue and Huseby [2002]

Two experiments from Grue and Huseby [2002] have been reproduced using IHFoam, the results are shown in fig. 5.22 and 5.23, with quite smooth wave forms. A good general agreement of the inline forces has been found on those. Secondary load cycles seem to show slightly just at the end of the primary load cycle, since this waves are not very steep. Coefficient  $cAlpha$  is set again to zero, to avoid artificial increase of steepness as discussed for previous cases.

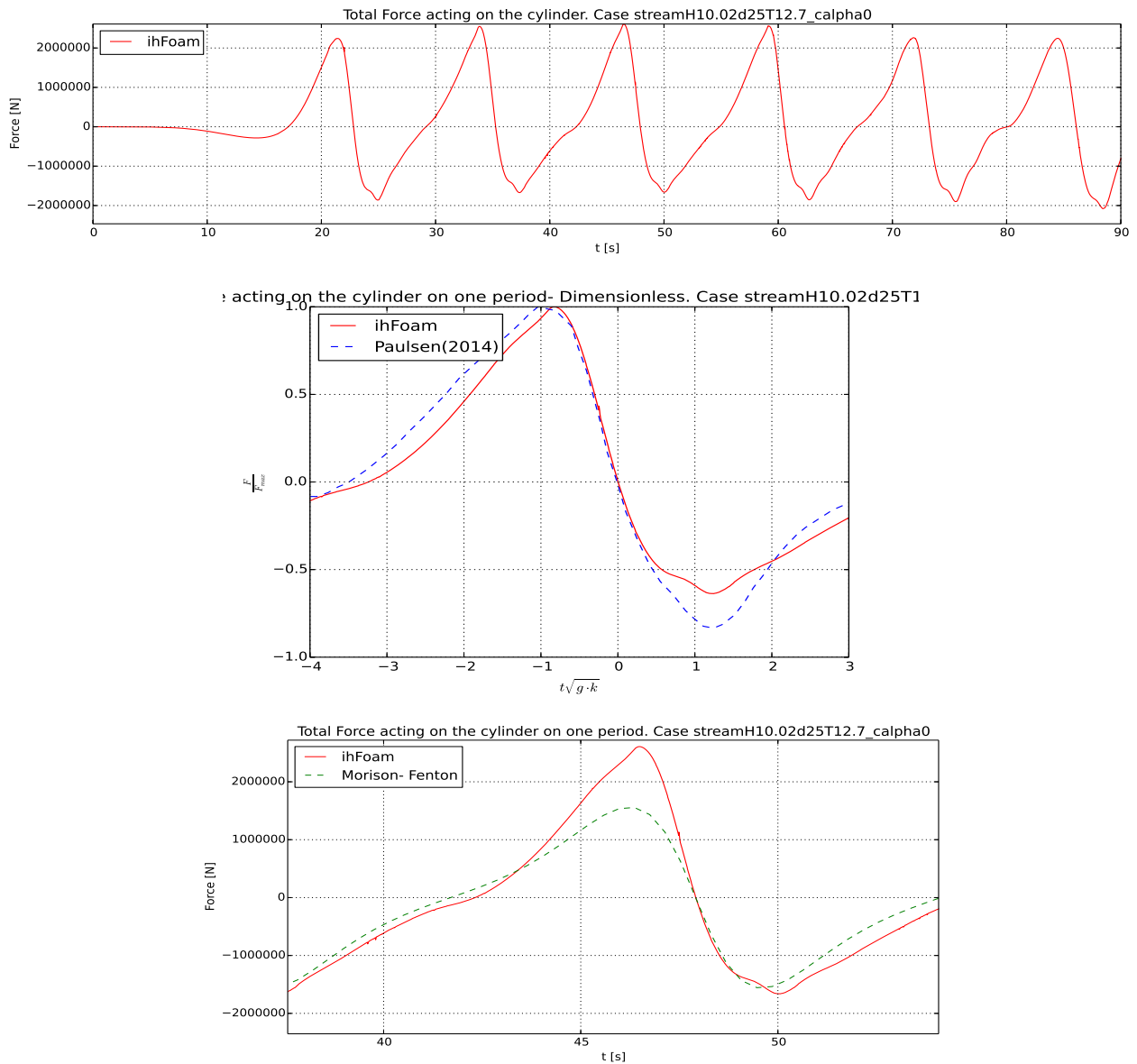


Figure 5.18: Inline forces on a cylinder of  $D=6$  m,  $H/H_{max}=0.6$ ,  $kd=0.85$  (Paulsen et al. [2012] table 1-case 2). Total simulation time (top), focus on one period compared with solution from Paulsen et al. [2012] (fig. 9) in dimensionless form (center) and comparison with Morison inertia forces derived from the accelerations in Fenton solution (bottom).

### 5.2.3 Load cycle

The time series obtained in this project for the wave loads on a vertical cylinder have some interesting features to highlight here, these are shown in figure 5.24. First there is clear vertical asymmetry on those plots, more pronounced in the steeper waves, the load profile increases to a maximum value just before the crest passes.

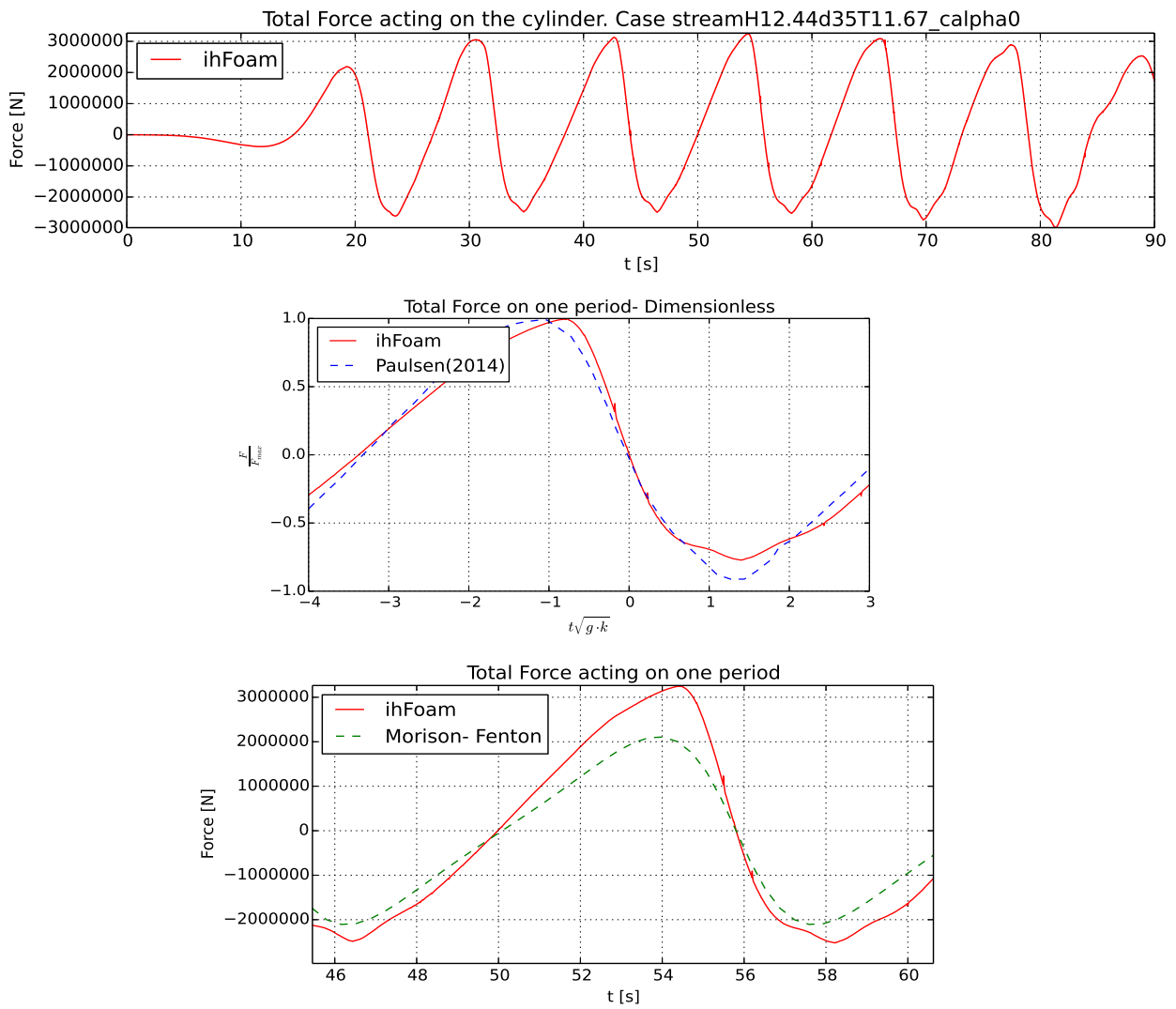


Figure 5.19: *Inline forces on a cylinder of  $D=6$  m,  $H/H_{max}=0.6$ ,  $kd=1.2$  (Paulsen et al. [2012] table 1-case 4). Total simulation time (top), focus on one period compared with solution from Paulsen et al. [2012] (fig. 9) in dimensionless form (center) and comparison with Morison inertia forces derived from the accelerations in Fenton solution (bottom).*

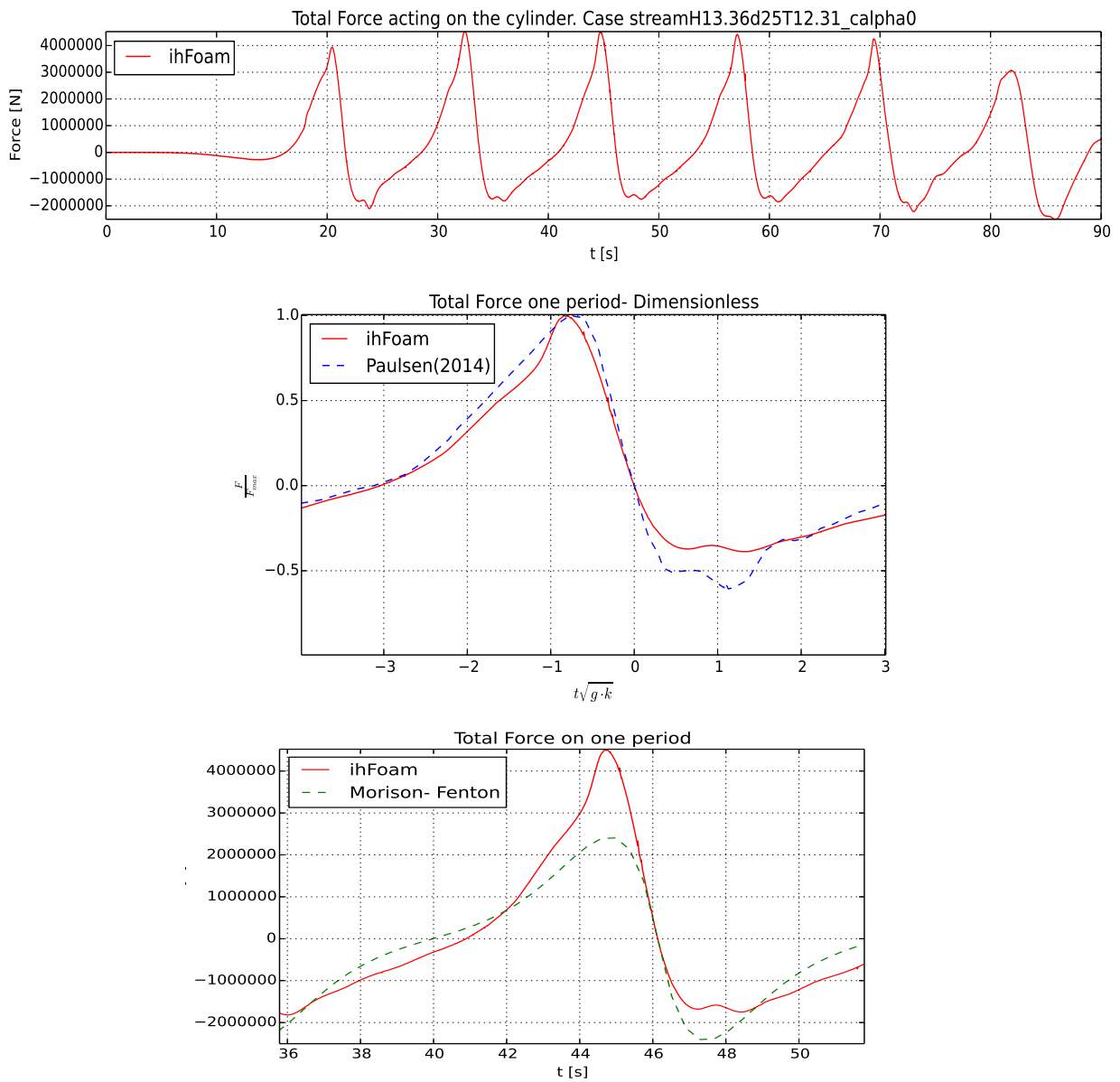


Figure 5.20: *Inline forces on a cylinder of  $D=6$  m,  $H/H_{max}=0.81$ ,  $kd=0.87$  (Paulsen et al. [2012] table 1-case 20). Total simulation time (top), focus on one period compared with solution from Paulsen et al. [2012] (fig. 9) in dimensionless form (center) and comparison with Morison inertia forces derived from the accelerations in Fenton solution (bottom).*

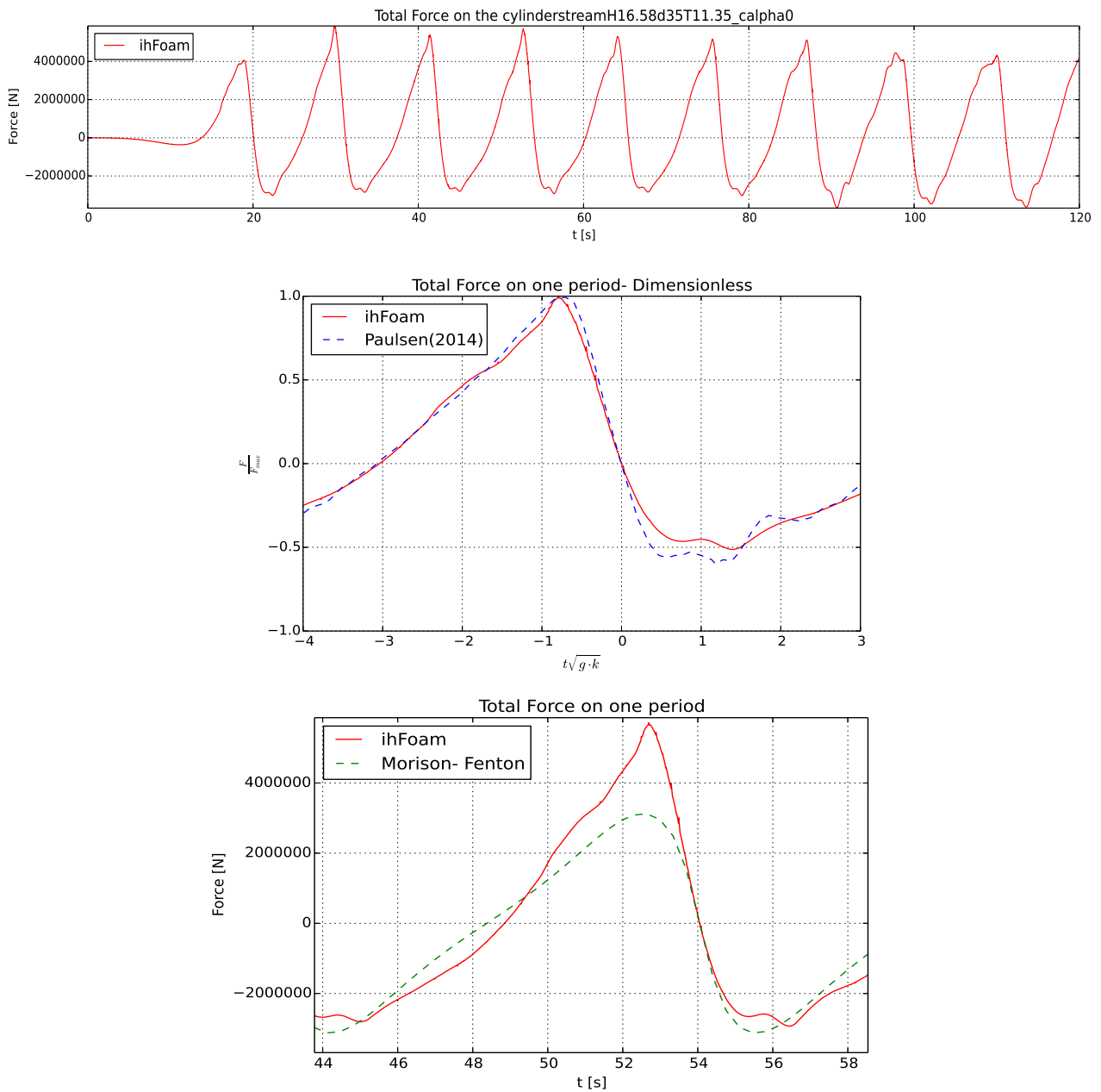


Figure 5.21: *Inline forces on a cylinder of  $D=6$  m,  $H/H_{max}=0.82$ ,  $kd=1.22$  (Paulsen et al. [2012] table 1-case 22). Total simulation time (top), focus on one period compared with solution from Paulsen et al. [2012] (fig. 9) in dimensionless form (center) and comparison with Morison inertia forces derived from the accelerations in Fenton solution (bottom).*



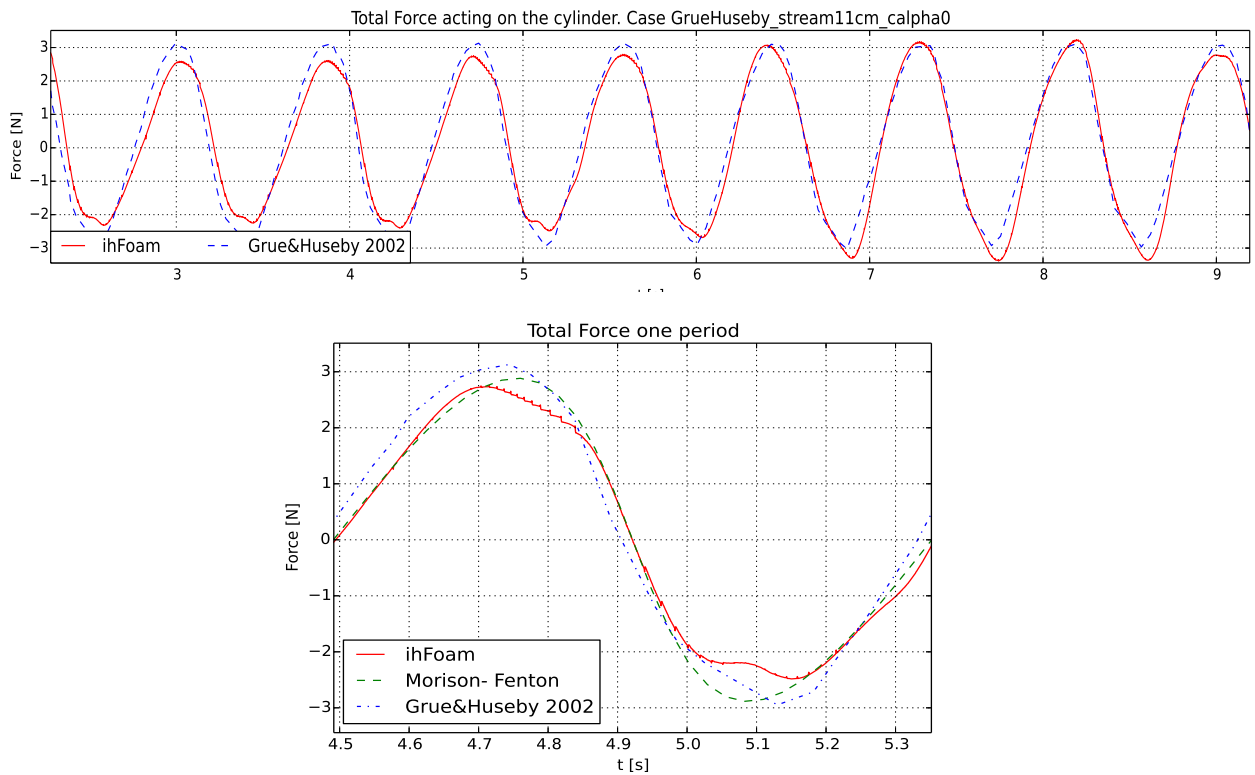


Figure 5.22: In-line forces on a cylinder of  $D=6$  cm,  $H/H_{max}=0.634$ ,  $kd=3.05$ . Total simulation time (top), focus on one period compared with experiments from Grue and Huseby [2002] and with Morison inertia forces derived from the accelerations in Fenton solution (bottom).

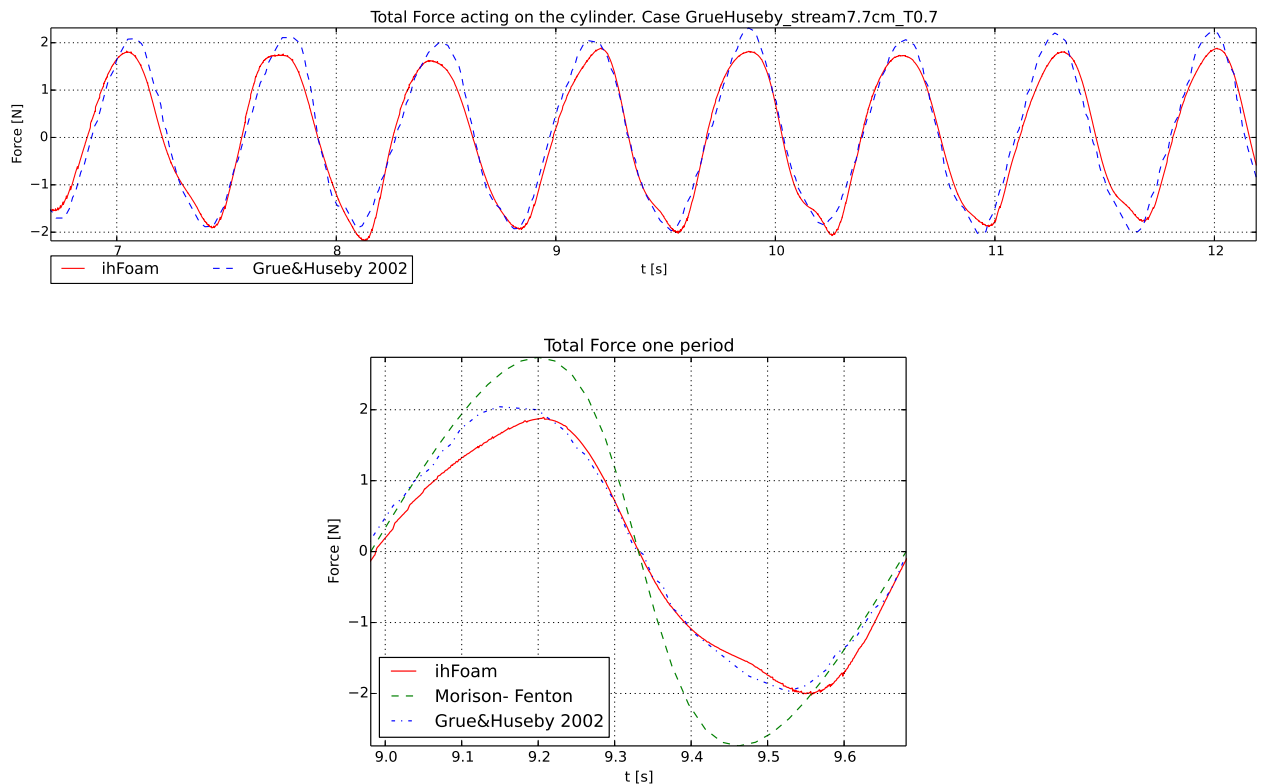
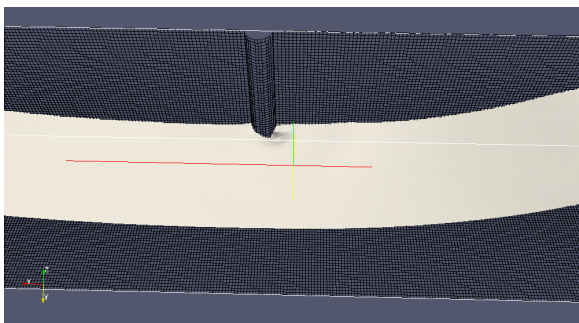
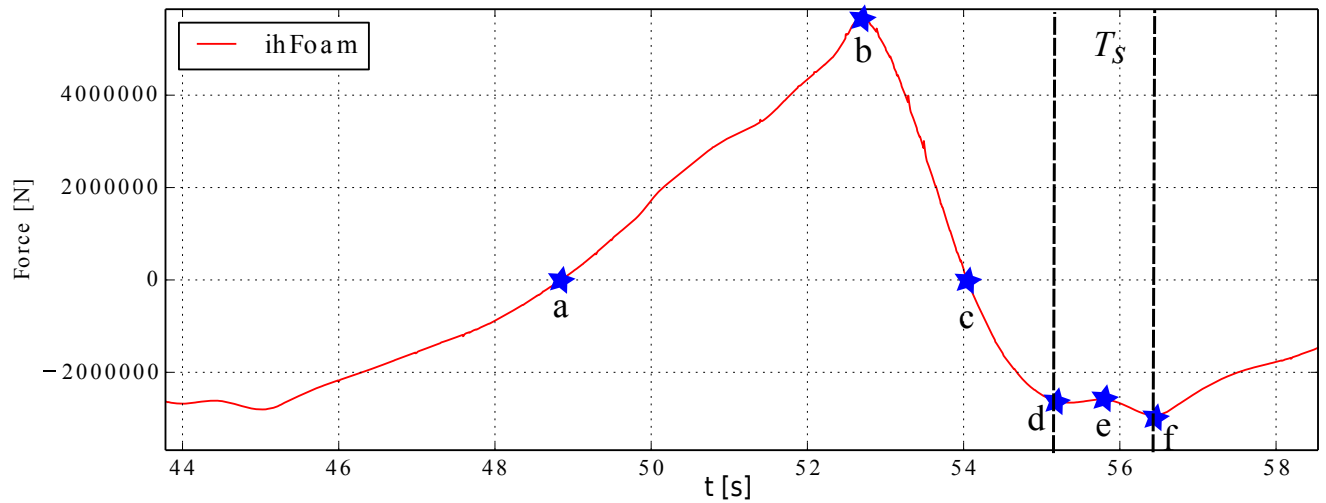
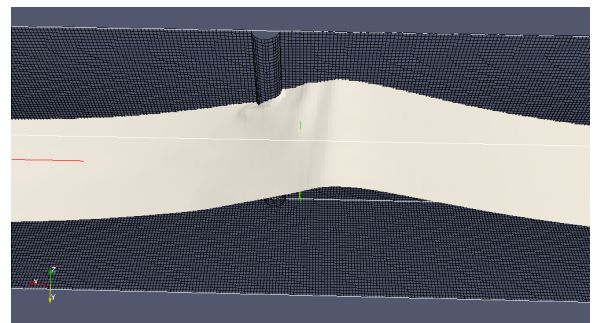


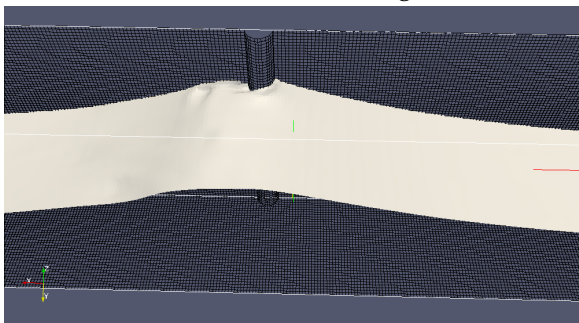
Figure 5.23: In-line forces on a cylinder of  $D=6$  cm,  $H/H_{max}=0.653$ ,  $kd=4.53$ . Total simulation time (top), focus on one period compared with experiments from Grue and Huseby [2002] and with Morison inertia forces derived from the accelerations in Fenton solution (bottom).



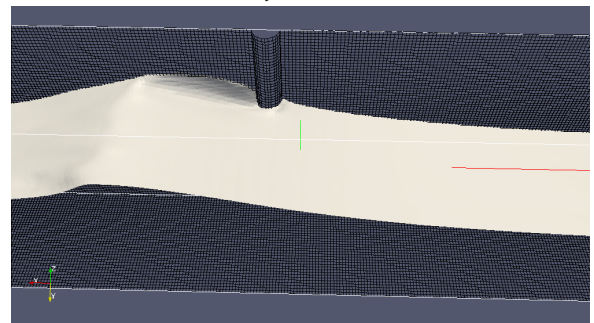
a) Zero inline force at through,  $t=48.9$  s



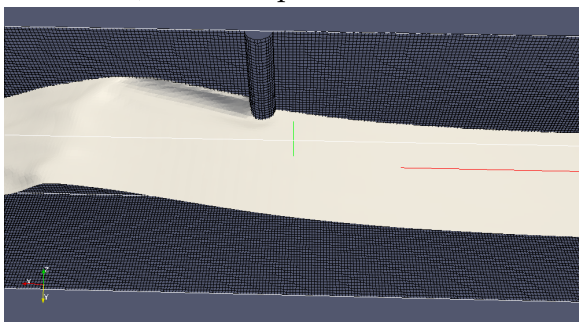
b) Maximum force just before crest,  $t=52.7$  s



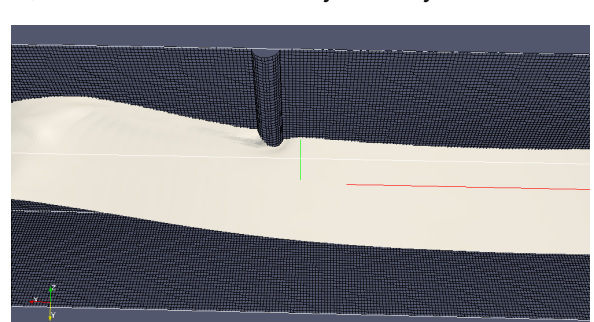
c) Force drop to 0,  $t=54.0$  s



d) Initiation of secondary load cycle,  $t=55.3$  s



e) Peak of secondary load cycle, diffracted wave gets to the symmetry plane,  $t=55.8$  s



f) End of secondary load cycle,  $t=56.5$  s

Figure 5.24: Images from one of the simulated cases on a cylinder of  $D=6$  m,  $T=11.35$  s,  $H/H_{max}=0.82$ ,  $kd=1.22$ . Inline force on one period (top), simulation screenshots (a-f).  $T_s$  is the period of the secondary load cycle, estimated here as 1.2 s.

## Chapter 6

# Summary and Conclusions

An overview of the state of the art of CFD simulation of waves is made in this report reviewing the theory and concepts to the state of the art of today's model. The the main challenges to achieve a realistic wave tank for further studies related to wave-structure interaction have also been highlighted.

Two dimensional wave flume simulations were investigated for a wide range of conditions to test the capability of IHFoam to predict wave forms and velocity profiles according to theory. All the simulations neglect the friction with walls and bottom, thus the turbulence model is set to laminar, and slip boundary conditions are included for all walls. This is consistent with theory since all the  $N_{KC} < 15$ .

Wave generation perform reasonably well for smooth waves, but fails to accurately represent Deficient wave generation on very steep waves causing instabilities in the wave profile. This is partially solved if the compression term from eq. 2.34 is removed.

The limits to the performance of the active absorption boundary condition are established based on the error of the simulations and the reflection at the boundaries. The active absorption boundary condition performs better for shallow to intermediate water depths  $L/d > 0.5$  with reflection coefficients that can get as low as 4.4% for steepness  $H/L = 0.05$  in intermediate depths ( $d/L = 0.1$ ); grow up to 22.4% in the limit of deep water conditions ( $d/L = 0.5$ ) and 68.9% if the waves go into very deep water ( $d/L = 2.29$ ). This greatly limits the applicability of this tool to model offshore conditions, specially in big depths. As an example, a design wave of around 20 m and  $T=14$  s will have  $L = \frac{gT^2}{2\pi} = 306m$ , deep water conditions implies that  $d > L/2 = 150m$  which is quite a low limit and is outbouded in many current offshore facilities, not to talk about the ultra deep water facilities that are to come.

The simulations show non linear effects on most cases, leading to an early breaking in some simulations–, approximately when  $H/L > 0.05$ – if the compression technique from eq. 2.34 is applied to the velocities. That is much before the predicted theoretical limit stated in [Fenton, 1990].

Another observed effect is that non linearities on the outlet patch, such as asymmetries, splashes and partially breaking waves, fail to be cancelled by the active absorption boundary condition, producing reflections in different frequencies than that of the harmonics of the incident wave. This is observed in all of the cases to a certain extent, but is more apparent in the OC5 set, where the periods are short (1-2 sec) and in very deep water conditions (see fig. 5.10). These non linear reflections are difficult to quantify, since the theory behind the obtention of the reflection coefficients relies in the applicability of the superposition principle form linear theory (see section 3.0.2) , which is not applicable in non linear systems. Non linear superposition of frequencies from wave runups and partial breaking of waves needs to be included in the active boundary condition if it aims the analysis of steep waves interaction with structures, specially with short periods.

Other artificial phenomenon is that of the spurious velocities induced by the active wave absorption boundary condition, tailored for shallow water, seem to induce a constant velocity profile  $U_c$  at the outlet, that might be propagating throughout the domain. The effect of this velocity in the generated waves is similar to that of an opposing current applied to a wave: it induces an increase in the steepness, and can cause early wave breaking [Wolf and Prandle, 1999]. This opposing current can be observed in fig. 5.14.

Another anomalous effect is that of the spurious high air velocities just above the interface and air blows from the outlet boundary, which can be of a concern if the velocities of the air phase are being looked into – i.e. for wind energy purposes.

This spurious effect has no clear solution since the cause lies within the VOF method and the absorption boundary condition implementation, [Afshar, 2010] proposes a relaxation of the velocities just above the water surface. Patterson [2008] proposed removing the convection term of the air phase above the free surface, modifying the air convection in the transport equation multiplying the convective term by the phase fraction value, so this is unmodified for the water phase ( $\alpha = 1$ ) and reduced for the partially filled and dry cells. Of course, none of those aim to accurately represent the air velocities above the wave, they just intend to avoid spurious effects of the air velocities on the wave. A more detailed work is needed to assess those solutions.

At the outlet boundary spurious air currents are also observed, maybe due to the fact that the active absorption boundary condition creates a cancellation velocity  $U_c$  – meant to affect the water phase – that also affects the air phase in the partially filled cells at the interface, creating a momentum that drives a velocity at the air phase that is about three times higher than  $U_c$ , due to the differences in density. This needs to be treated numerically within the absorption boundary condition, maybe including similar solutions as the ones presented by [Afshar, 2010] and Patterson [2008].

It looks like tailoring an absorption boundary condition for a general case is a cumbersome task. The active boundary condition implemented in IHFoam performs well under some circumstances, that is, shallow to intermediate water depths (reflections less than 10% when  $d/L < 0.16$ ) with little non linearities involved, since it is based on linear theory. Skewed wave forms, splashes, near breaking or breaking waves won't be cancelled by the boundary condition, which will try to approximate the water elevation to a linear wave form reflected back from the outlet to generate the cancelling velocity  $U_c$  field.

Three dimensional simulations, including a vertical cylinder in the middle of the flume, are included as a second phase of the project for completeness. Forces are calculated based on a frictionless approach, ensuring that all cases are inertia dominated and drag forces can be neglected.

The time series for the loads are obtained removing the compression term so to avoid early breaking. They all show similar patterns than those shown in Paulsen et al. [2012]: Smoother waves, with steepness  $H/L < 0.068$ , show round-shaped, sinusoidal like, force profiles; steeper cases show a saw-tooth profile with acute peaks, suggesting wave asymmetries and some slamming forces, with forces greater than those predicted by Morison equation. Secondary load cycles show after the maximum load peak, appearing in all cases, slightly showing up in less steep waves ( $H = 0.6H_{max}$ ), earlier than those obtained by the referred author ( $H = 0.8H_{max}$ ), but this is not regarded as a big concern since the overall agreement is good.

Agreement with Grue and Huseby [2002] experiments is very good, since those two cases are based on smooth profiles. The error here is very small, less than 5%, and the model is able to represent accurately the main features of the measured time series (peak, phase, secondary cycle).

## 6.1 Further work

Further work needs to be carried out in relation to the develop of active absorption boundary conditions valid for a wide range of conditions, [Wellens \[2012\]](#) work is a good base to do so. They should be able to cancel a wide range of reflected frequencies coming from non linearities and perform well in deep water, specially for offshore applications.

Another important field for improvement is the inclusion of realistic wind velocities in the air phase. It has not been set focus on this aspect here but it can be of importance in the case of wind wave interaction and generation of waves, or in the context of wind turbine projects, for instance. Coinciding with the observations by [Afshar \[2010\]](#), the VOF method seems to be including artificially high velocities at the interface.

Others fields of research is the inclusion of a turbulence model (such as  $\kappa - \epsilon$  or *LES*) and modelling a boundary layer around the cylinder to simulate drag force, so the work can be extended to higher Keulegan-Carpenter numbers.

It would also be interesting to see a thorough study of the accuracy of the model to predict wave breaking and wave slamming loads, validated both against experiments and theory (based on eq. [2.26](#), for instance). The numerical modelling of waves and its validation through theory and experiments is limited because all three methods –theory, experiments and numerical modelling – have their inaccuracies, assumptions and drawbacks. Experiments have lack of control over all parameters, such as accurate wave generation and absorption, theory usually has too limiting assumptions regarding non linearities, interaction with the atmosphere and friction, and numerical methods rely on input from those two.

# Bibliography

*Waves in Fluids*, p. 205. Cambridge University Press, 2001.

*Ocean Waves Breaking and Marine Aerosol Fluxes*. Springer Science & Business Media, p. 12, 2007.

M. A. Afshar. Numerical wave generation in openfoam. Master's thesis, Chalmers University of Technology, 2010.

E. Berberović, N. Van Hinsberg, S. Jarkirlić, I. Roisman, and C. Tropea. Drop impact onto a liquid layer of finite thickness: dynamics of the cavity evolution. *Physical Review*, E 79 036306, 2009.

J. R. Chaplin. Hydrodynamic damping of a cylinder at  $\beta \approx 10^6$ . *Journal of Fluids and Structures*, 14: 1101–1117, 2000.

Edinburgh Designs Limited. Beach design-absorbing beaches. URL <http://www.edesign.co.uk/waves/beach-design/>.

J. D. Fenton. Nonlinear wave theories. In Eds. B. Le Méhauté and New York D.M. Hanes, Wiley, editors, *The Sea, Vol.9: Ocean Engineering Science*, pages 9–25. 1990. URL <http://johndfenton.com/Papers/Fenton90b-Nonlinear-wave-theories.pdf>.

J.D. Fenton and M.M. Rienecker. A fourier method for solving nonlinear water-wave problems: application to solitary-wave interactions. *Journal of Fluid Mechanics*, 118:411–443, 1982.

John D. Fenton. *Fourier and Stokes software*, March 2014. URL <http://johndfenton.com/Steady-waves/Fourier.html>.

Yoshimi Goda and Tasumasa Suzuki. Estimation of incident and reflected waves in random wave experiments. *Coastal Engineering Proceedings*, 1(15), 2011. ISSN 2156-1028. URL <https://icce-ojs-tamu.tdl.org/icce/index.php/icce/article/view/3096>.

J. Grue and M. Huseby. On higher harmonic wave loads on vertical cylinders and ringing of offshore structures. In *17th International Workshop on Water Waves and Floating Bodies*, Cambridge, UK, April 2002.

P. Hall. On the stability of the unsteady boundary layer on a cylinder oscillating transversely in a viscous fluid. *Journal of Fluid Mechanics*, 146:347–367, 1984.

P. Higuera, J. L. Lara, and I. J. Losada. Realistic wave generation and active wave absorption for navier–stokes models: Application to openfoam. *Coastal Engineering, Vol. 71, pp. 102-118.*, 2013.

C. Hirt and B. Nichols. Volume of fluid (vof) method for the dynamics of free boundaries. *Journal of Computational Physics*, 39:201–225, 1981.

H. Honji. Streaked flow around an oscillating circular cylinder. *Journal of Fluid Mechanics*, 107:509–520, 1981.

M. Huseby and J. Grue. An experimental investigation of higher-harmonic wave forces on a vertical cylinder. *Journal of Fluid Mechanics*, 414:75–103, 2000.

- Niels G. Jacobsen, David R. Fuhrman, and Jørgen Fredsøe. A wave generation toolbox for the open-source cfd library: Openfoam®. *International Journal for Numerical Methods in Fluids*, 70(9):1073–1088, 2012. ISSN 1097-0363. doi: 10.1002/flid.2726. URL <http://dx.doi.org/10.1002/flid.2726>.
- R. Luppés, Veldman, A.E.P., and P.R. Wellens. Absorbing boundary conditions for wave simulations around offshore structures. In *Proceedings ECCOMAS CFD 2010 Paper 1200*, 2010.
- F.J. Mendez, I.J. Losada, and M.A. Losada. Wave-induced mean magnitudes in permeable submerged breakwaters. *Journal of Waterway, Port, Coastal, and Ocean Engineering*, (127):7–15, 2001.
- B. Le Méhauté. *Introduction to Hydrodynamics and Water Waves*. Springer-Verlag, 1976.
- A. Otter. Damping forces on a cylinder oscillating in a viscous fluid. *Applied Ocean Research*, 12: 153–155, 1990.
- E. Patterson. Multiphase and free surface flow simulations. "Presented at Third OpenFOAM® Workshop. Politecnico di Milano, Milan, Italy", 2008.
- B. T. Paulsen, H. Bredmose, and H. B. Bingham. Accurate computation of wave loads on a bottom fixed circular cylinder. *International Workshop on Water Waves and Floating Bodies*, 2012.
- Zhong Peng. Wave slamming impact on offshore wind turbine foundation. *Coastal Engineering*, 2014.
- T. Sarpkaya. Force on a circular cylinder in viscous oscillatory flow at low keulegan-carpenter numbers. *Journal of Fluid Mechanics*, 165:61–71, 1986.
- H.A. Schäffer and G. Klopman. Review of multidirectional active wave absorption methods. *Journal of Waterway, Port, Coastal, and Ocean Engineering*, pages 88–97, April 2000.
- G. G. Stokes. *On the effect of the internal friction of fluids on the motion of pendulums*, volume 9, pages 8–106. Transactions of the Cambridge Philosophical Society, 1851.
- B. M. Sumer and J. Fredsø. Hydrodynamics around cylindrical structures. *World Scientific*, 2006.
- F. C. K. Ting and J. T. Kirby. Observations of undertow and turbulence in a laboratory surfzone. *Coastal Engineering*, 24:51–80, 1994.
- C. Y. Wang. On high-frequency oscillatory viscous flows. *Journal of Fluid Mechanics*, 32:55–68, 1968.
- G. Wei and J.T. Kirby. Time-dependent numerical code for extended boussinesq equations. *Journal of Waterway, Port, Coastal, and Ocean Engineering*, (121):251–261, 1995.
- P. R. Wellens. *Wave Simulation in Truncated Domains for Offshore Applications*. PhD thesis, Technical University of Delft, 2012.
- H. G. Weller, G. Tabor, H. Jasak, and C. Fureby. A tensorial approach to computational continuum mechanics using object-oriented techniques. *Computer Physics*, 12(6), 1998.
- H.G. Weller. Derivation, modelling and solution of the conditionally averaged two-phase flow equations. Technical report, R/HGW/02. Nabla Ltd, 2002.
- J. M. Williams. Limiting gravity waves in water of finite depth. *Philosophical Transactions of the Royal Society of London. Series A, Mathematical and Physical Sciences*, 302(1466):pp. 139–188, 1981. URL <http://www.jstor.org/stable/36960>.
- J. Wolf and D. Prandle. Some observations of wave–current interaction. *Coastal Engineering*, 37:471–485, 1999.